博士論文

Pairing Interactions Mediated by Ferromagnetic Magnons
―Odd- and Even-Frequency Superconductivities―

（強磁性マグノンが媒介する
対形成相互作用
―奇周波数及び偶周波数超伝導―）

舟木　博志

広島大学大学院先端物質科学研究科

2015 年 3 月

目次

主論文

Acknowledgements

I would like to express my deep gratitude to Professor Hiroshi Shimahara for his continuous support and valuable advises. I would also like to express my thanks to Dr. Arata Tanaka, Professor Katsuhiko Higuchi, and Dr. Tatsuya Shishido for their encouragement. I am grateful to Mr. Kazuhiro Ito and all members of Institute of Theoretical Physics for their encouragement.

Contents

Chapter 1

Introduction

1.1 Overview and purpose of the study

In connection with exotic superconductors, such as heavy-fermion, organic, copper oxide and iron pnictide superconductors, superconductivity mediated by magnetic fluctuations has been studied extensively. Magnetic order and magnetic tendency of the systems dominate the nature of superconductivity in those materials. For example, in ferromagnetic superconductors, strong exchange field suppresses the antiparallel spin pairing. Relation between superconductivity and ferromagnetism has been studied in $ErRh_4B_4$ [1,2] and $HoMo_6S_6$ [3,4], in which the spin moments that exhibit ferromagnetic order are considered to be localized. In these compounds, however, it has been revealed that superconductivity and ferromagnetism do not coexist in microscopic scale. In recent years, microscopic coexistence of superconductivity and ferromagnetism has been observed in UGe_2 [5], URhGe [6], and UCoGe [7], in which the electrons responsible for the ferromagnetic order are itinerant [8]. Following these observations, superconductivity mediated by ferromagnetic fluctuations has been examined.

With these experimental and theoretical studies as motivations, we investigate superconductivity mediated by ferromagnetic fluctuations in this thesis. We assume the generalized Kondo lattice model in which the ferromagnetic order occurs in a localized spin system. We derive the effective interactions between conduction electrons by the perturbation theory. In quasi-one dimension, we numerically calculate the pairing susceptibility, fully taking into account the spatial and temporal dependences.

When the magnetic order is established, magnetic fluctuations around the long-range order are expressed in terms of magnons. As pointed out by many authors [9–12], magnons can mediate effective interactions between electrons, which may induce superconductivity. In ferromagnetic superconductors, magnon-exchange mechanism of superconductivity was examined by Kerchev et al. [10]. Assuming antiparallel spin pairing, they obtained a linear temperature dependence of specific heat at low temperatures. Hattori and Tsunetsugu examined reentrant superconductivity in an Ising ferromagnetic superconductor URhGe in a transverse magnetic field [12]. Assuming the one-magnon-exchange interaction, they found that soft magnons generate strong attractive interactions near a transverse saturation field.

The interactions mediated by magnons are analogous to those mediated by phonons, but the magnon-exchange interactions have some specific features. First, the magnon-exchange interactions depend on the electron spins, because magnon carries spin angular momentum $-\hbar$, when spin quantization axis is parallel to the spontaneous magnetization. Only the spin-up electrons can absorb magnon, whereas only the spin-down electrons can emit magnon. Therefore, the one-magnon-exchange interaction contributes only to antiparallel spin pairing. Second, each electron can simultaneously absorb and emit magnons. This leads to the two-magnon-exchange interaction between two electrons and can induce both parallel and antiparallel spin pairings. In the antiferromagnetic case, superconductivity mediated by the one- and two-magnon-exchange interactions was examined by Shimahara [9]. It was found that either the d-wave spin-singlet state or the p-wave spin-triplet state is induced by magnon-mediated interactions, depending on the electron density of the system. In the ferromagnetic case, however, the two-magnon-exchange interaction vanishes in the limit $T \to 0$, in contrast to that in the antiferromagnetic case. Therefore, we need to proceed to the third order processes. The third order processes are described by the triangle processes of one electron and two magnon propagators. Below, we reveal that the triangle processes give the lowest order contribution to the effective interactions at low temperatures, and can induce both parallel and antiparallel spin pairings.

In the calculation of the pairing susceptibility, we need to fully account the temporal dependences, to examine both possibilities of odd- and even-frequency superconductivities. The odd-frequency superconductivity was first proposed by Berezinskii in a study of superfluid ^{3}He [13]. Later, some features of odd-frequency superconductivity were examined [14–17]. Describing the order parameter of odd-frequency superconductivity in term of the expectation value of a composite operator, Abrahams et al. [15] examined reentrant behavior, Meissner effect and some other properties. In heavy fermion compounds, Coleman et al. investigated this state [18]. Vojta and Dagotto also examined this state in triangular antiferromagnets [19]. In recent years, this state was studied in some other systems [20–22]. Odd-frequency superconductivity in ferromagnets was investigated in superconductor-ferromagnet structures [23–27]. The bulk mixed even- and odd-frequency superconductivity coexisting with ferromagnetism was examined by Matsumoto et al. [28]. Assuming the s-wave antiparallel spin pairing and the interactions mediated by the Einstein phonons, they elucidated the emergent mixing between even- and odd-frequency pairings.

1.2 Ferromagnetic superconductors

The first ferromagnetic superconductor UGe_2 was discovered by Saxena et al. [5]. The ferromagnetic transition temperature $T_{\rm FM}$ is 53 K at ambient pressure, and decreases as pressure P increases, and vanishes at $P \sim 1.6$ GPa. Superconductivity occurs only in the ferromagnetic phase where $1.0 \lesssim P \lesssim 1.6$ GPa. The superconducting transition temperature T_c becomes the maximum $T_c \sim 0.7$ K at $P \sim 1.5$ GPa. In URhGe discovered by Aoki et al. [6], superconductivity and ferromagnetism coexist at ambient pressure with $T_c \sim 0.25$ K and $T_{FM} = 9.5$ K. Huy et al. observed coexistence of ferromagnetic order and superconductivity in UCoGe [7]. They found $T_{FM} = 3$ K and $T_c \sim 0.8$ K at ambient pressure.

$ZrZn_2$ was examined by Pfleiderer et al. [29]. They determined the transition temperature as $T_c = 0.29$ K from a rapid drop of the electrical resistivity. Akazawa et al. examined UIr [30], and found that superconductivity occurs below $T_c = 0.14$ K, where $2.6 \lesssim P \lesssim 2.7$ GPa.

1.3 Pairing interactions mediated by ferromagnetic fluctuations

Since the investigation by Kohn and Lattinger [31], superconductivity induced by repulsive interactions has been examined by many authors. Berk and Schrieffer [32] and Nakajima [33] examined the pairing interaction mediated by paramagnon in nearly ferromagnetic Fermi liquids. Fay and Appel studied p-wave equal-spin pairing mediated by the longitudinal spin fluctuations both in paramagnetic and magnetic regions [34]. Later, in ferromagnetic superconductors, such as UGe_2, URhGe, and $ZrZn_2$, it was found that superconductivity occurs only in the ferromagnetic state. In connection with these experiments, Kirkpatrick et al. examined coupling of magnons to the longitudinal magnetic susceptibility [35]. Walker and Samokhin proposed an exchange-type interaction between the magnetic moments of spin triplet Cooper pairs in $ZrZn_2$ [36]. Nevidomskyy studied the effect of phase crossover from isotropic to uniaxial spin fluctuations near quantum phase transition [37]. In UCoGe, superconductivity occurs both in paramagnetic and magnetic regions. Tada et al. calculated upper critical field of spin-triplet superconductivity induced by longitudinal ferromagnetic fluctuations in UCoGe [38].

In this thesis, we adopt the generalized Kondo lattice model, to examine pairing interactions mediated by ferromagnetic fluctuations. In this model, the ferromagnetic long-range order occurs in the localized spin system, and superconductivity occurs in the itinerant electron system that is coupled with the localized spin system through the Kondo coupling. This state is different from those of the models in the previous studies. In case that we apply the present theory to the compounds mentioned above, this is a simplification, but allows us to approach the problem in a simpler way analogous to the phonon mediated pairing interactions. Hence, we can develop the theory more systematically using the perturbation theory. Furthermore, we can elucidate the difference between the phonon- and magnon-mediated pairing interactions in this approach. Below, we reveal the specific features of the pairing interactions mediated by ferromagnetic spin fluctuations on the basis of this model.

1.4 Odd-frequency superconductivity

In this subsection, we briefly explain the odd-frequency superconductivity. The anomalous Green's function is defined as

$$\mathcal{F}_{\sigma\bar{\sigma}}(\boldsymbol{k},\omega_n) = \int_0^\beta d\tau e^{i\omega_n\tau}\langle\mathcal{T}[c_{\boldsymbol{k}\sigma}(\tau)c_{-\boldsymbol{k}\bar{\sigma}}]\rangle, \tag{1.1}$$

where $\beta = 1/T$ and $\omega_n = \pi T(2n+1)$. Thus, we obtain

$$\begin{aligned}
\mathcal{F}_{\bar{\sigma}\sigma}(-\boldsymbol{k},-\omega_n) &= \int_0^\beta d\tau e^{-i\omega_n\tau}\langle\mathcal{T}[c_{-\boldsymbol{k}\bar{\sigma}}(\tau)c_{\boldsymbol{k}\sigma}]\rangle \\
&= -\int_0^{-\beta} d\tau e^{i\omega_n\tau}\langle\mathcal{T}[c_{-\boldsymbol{k}\bar{\sigma}}(-\tau)c_{\boldsymbol{k}\sigma}]\rangle \\
&= -\int_0^{\beta} d\tau e^{i\omega_n\tau}\langle\mathcal{T}[c_{\boldsymbol{k}\sigma}(\tau)c_{-\boldsymbol{k}\bar{\sigma}}]\rangle \\
&= -\mathcal{F}_{\sigma\bar{\sigma}}(\boldsymbol{k},\omega_n).
\end{aligned} \tag{1.2}$$

Below, we define the anomalous Green's functions for spin-singlet and triplet pairings as

$$\mathcal{F}_{\mathrm{sin}}(\boldsymbol{k},\omega_n) = \frac{1}{\sqrt{2}}[\mathcal{F}_{\uparrow\downarrow}(\boldsymbol{k},\omega_n) - \mathcal{F}_{\downarrow\uparrow}(\boldsymbol{k},\omega_n)] \tag{1.3}$$

and

$$\mathcal{F}_{\rm tri}(\boldsymbol{k},\omega_n) = \frac{1}{\sqrt{2}}[\mathcal{F}_{\uparrow\downarrow}(\boldsymbol{k},\omega_n) + \mathcal{F}_{\downarrow\uparrow}(\boldsymbol{k},\omega_n)], \tag{1.4}$$

respectively. From Eq. (1.2),

$$\mathcal{F}_{\rm sin}(-\boldsymbol{k},-\omega_n) = \mathcal{F}_{\rm sin}(\boldsymbol{k},\omega_n) \tag{1.5}$$

and

$$\mathcal{F}_{\rm tri}(-\boldsymbol{k},-\omega_n) = -\mathcal{F}_{\rm tri}(\boldsymbol{k},\omega_n). \tag{1.6}$$

If the system has the time-reversal and parity symmetries, $\mathcal{F}_{\rm sin}(\boldsymbol{k},\omega_n)$ and $\mathcal{F}_{\rm tri}(\boldsymbol{k},\omega_n)$ satisfy

$$\mathcal{F}_{\rm sin}(\boldsymbol{k},\omega_n) = \pm\mathcal{F}_{\rm sin}(-\boldsymbol{k},\omega_n) = \pm\mathcal{F}_{\rm sin}(\boldsymbol{k},-\omega_n) \tag{1.7}$$

and

$$\mathcal{F}_{\rm tri}(\boldsymbol{k},\omega_n) = \pm\mathcal{F}_{\rm tri}(-\boldsymbol{k},\omega_n) = \mp\mathcal{F}_{\rm tri}(\boldsymbol{k},-\omega_n), \tag{1.8}$$

respectively.

The order parameter is defined by

$$\Delta(\boldsymbol{k},\omega_n) = \sum_{\boldsymbol{k}',n'} \Gamma(\boldsymbol{k},\omega_n,\boldsymbol{k}',\omega_{n'})\mathcal{F}(\boldsymbol{k}',\omega_{n'}), \tag{1.9}$$

where Γ is the effective pairing interaction. Therefore, $\Delta(\boldsymbol{k},\omega_n)$ and $\mathcal{F}(\boldsymbol{k},\omega_n)$ have the same symmetry. When $\mathcal{F}(\boldsymbol{k},\omega_n)$ is an odd function of ω_n, the superconducting order is called odd-frequency superconductivity. We summarize the classification of superconducting order parameters in Table 1.1. Thus, odd-frequency superconductivity is classified into odd-parity spin-singlet pairing and even-parity spin-triplet pairing. In recent years, Fuseya et al. [20] and Shigeta et al. [21] examined p-wave singlet pairing. Kusunose et al. [22] examined s-wave triplet pairing in strong-coupling electron-phonon systems. In this thesis, we examine parallel spin pairing, because strong exchange field suppresses the antiparallel spin pairing. We reveal that even-parity triplet pairing can be induced by the effective interactions mediated by magnons.

	Even-frequency $\Delta(\boldsymbol{k},\omega_n) = +\Delta(\boldsymbol{k},-\omega_n)$	**Odd-frequency** $\Delta(\boldsymbol{k},\omega_n) = -\Delta(\boldsymbol{k},-\omega_n)$
Even-parity $\Delta(\boldsymbol{k},\omega_n) = +\Delta(-\boldsymbol{k},\omega_n)$	**Singlet** $\uparrow\downarrow - \downarrow\uparrow$	**Triplet** $\uparrow\uparrow, \downarrow\downarrow, \uparrow\downarrow + \downarrow\uparrow$
Odd-parity $\Delta(\boldsymbol{k},\omega_n) = -\Delta(-\boldsymbol{k},\omega_n)$	**Triplet** $\uparrow\uparrow, \downarrow\downarrow, \uparrow\downarrow + \downarrow\uparrow$	**Singlet** $\uparrow\downarrow - \downarrow\uparrow$

Table 1.1: Classification of superconducting order parameters.

Chapter 2

Model and Formulation

2.1 Generalized Kondo lattice model and fermion-magnon model

We start from the generalized Kondo lattice model

$$\mathcal{H} = \mathcal{H}_t + \mathcal{H}_J + \mathcal{H}_\mathrm{K} \tag{2.1}$$

with

$$\mathcal{H}_t = \sum_{i,j,\sigma} t_{ij} {c_{i\sigma}}^\dagger c_{j\sigma} - \mu \sum_{i,j,\sigma} {c_{i\sigma}}^\dagger c_{i\sigma} \tag{2.2}$$

$$\mathcal{H}_J = - \sum_{(i,j),\alpha} J^\alpha S_i^\alpha S_j^\alpha \tag{2.3}$$

$$\mathcal{H}_\mathrm{K} = \sum_{i,\alpha} J_\mathrm{K}^\alpha S_i^\alpha s_i^\alpha, \tag{2.4}$$

where $\alpha = x, y, z$, the summation $\sum_{(i,j)}$ is over nearest-neighbor sites, and S_i^α is a localized spin operator on site i. We have defined

$$s_i^\alpha = \frac{1}{2} \sum {c_{i\sigma_1}}^\dagger \sigma^\alpha_{\sigma_1\sigma_2} c_{j\sigma_2}, \tag{2.5}$$

where σ^α denote the Pauli matrices. This model is a generalized version of the Kondo lattice model, which contains the exchange coupling J between the localized spins. We define $J^\perp \equiv J^z$, $J^\parallel \equiv J^x = J^y$, $J_{\mathrm{K}}^\perp \equiv J_{\mathrm{K}}^z$, $J_{\mathrm{K}}^\parallel \equiv J_{\mathrm{K}}^x = J_{\mathrm{K}}^y$, and $J^\parallel > J^\perp > 0$ for ferromagnets.

Adopting the Holstein-Primakoff transformation [39] for the localized spin system:

$$S_i^z = S - \hat{n}_i, \tag{2.6}$$

$$S_i^- = a_i^\dagger (2S - \hat{n}_i)^{\frac{1}{2}}, \tag{2.7}$$

$$S_i^+ = (2S - \hat{n}_i)^{\frac{1}{2}} a_i, \tag{2.8}$$

we derive fermion-magnon model. At sufficiently low temperatures in comparison to the ferromagnetic transition temperature T_{FM}, because $n_i \equiv \langle \hat{n}_i \rangle \ll S$, we can approximate Eqs. (2.7) and (2.8) as

$$S_i^- \approx \sqrt{2S} a_i^\dagger, \tag{2.9}$$

$$S_i^+ \approx \sqrt{2S} a_i, \tag{2.10}$$

respectively. Therefore, we obtain

$$\mathcal{H}_J \approx -J^\parallel S^2 \frac{Nz}{2} - \sum_{i,\boldsymbol{\rho}} \Big(-J^\parallel S \hat{n}_i + J^\perp S a_{i+\boldsymbol{\rho}}^\dagger a_i \Big) \equiv \mathcal{H}_{\mathrm{sw}}, \tag{2.11}$$

where N and z are the numburs of all localized spin sites and nearest-neighbor sites, respectively. Ignoring forth-order terms of magnon operators, Hamiltonian Eq. (2.11) is diagonalized by the Fourier transformation as

$$\mathcal{H}_{\mathrm{sw}} = -J^\parallel S^2 \frac{Nz}{2} + J^\parallel S z \sum_{\boldsymbol{q}} \Big(1 - \frac{J^\perp}{J^\parallel} \gamma(\boldsymbol{q}) \Big) a_{\boldsymbol{q}}^\dagger a_{\boldsymbol{q}}, \tag{2.12}$$

with

$$\gamma(\boldsymbol{k}) = \frac{1}{z} \sum_{\boldsymbol{\rho}} e^{\mathrm{i}\boldsymbol{k}\cdot\boldsymbol{\rho}}. \tag{2.13}$$

Because the first term of the right hand side of Eq. (2.12) is constant, we omit it below. The second term is the Hamiltonian for the magnon excitation energy, which becomes gapless if $J^{\perp} = J^{\parallel}$. In a similar way, we obtain

$$\mathcal{H}_{\mathrm{K}} = \sum_i \Big[J_{\mathrm{K}}^{\parallel}\ (S - \hat{n}_i)\frac{1}{2}(c_{i\uparrow}^{\dagger}c_{i\uparrow} - c_{i\downarrow}^{\dagger}c_{i\downarrow}) + J_{\mathrm{K}}^{\perp}\frac{\sqrt{2S}}{2}(a_i c_{i\downarrow}{}^{\dagger}c_{i\uparrow} + a_i^{\dagger}c_{i\uparrow}{}^{\dagger}c_{i\downarrow})\Big]. \tag{2.14}$$

We call $\mathcal{H}_t + \mathcal{H}_{\mathrm{sw}} + \mathcal{H}_{\mathrm{K}}$ the fermion-magnon model. Equation (2.14) is divided into three parts as

$$\mathcal{H}_{\mathrm{K}}^{z0} = \frac{J_{\mathrm{K}}^{\parallel}S}{2}\sum_i (c_{i\uparrow}^{\dagger}c_{i\uparrow} - c_{i\downarrow}^{\dagger}c_{i\downarrow}) \tag{2.15}$$

$$\mathcal{H}_{\mathrm{K}}^{xy} = J_{\mathrm{K}}^{\perp}\sqrt{\frac{S}{2}}\sum_i (a_i c_{i\downarrow}{}^{\dagger}c_{i\uparrow} + a_i^{\dagger}c_{i\uparrow}{}^{\dagger}c_{i\downarrow}) \tag{2.16}$$

$$\mathcal{H}_{\mathrm{K}}^{z} = -\frac{J_{\mathrm{K}}^{\parallel}}{2}\sum_i a_i^{\dagger}a_i(c_{i\uparrow}^{\dagger}c_{i\uparrow} - c_{i\downarrow}^{\dagger}c_{i\downarrow}). \tag{2.17}$$

$\mathcal{H}_{\mathrm{K}}^{z0}$ describes the exchange field for the conduction electrons, which is created by the localized spins. $\mathcal{H}_{\mathrm{K}}^{xy}$ describes absorption and emission of magnons by electrons. $\mathcal{H}_{\mathrm{K}}^{z}$ describes simultaneous absorption and emission of magnons by electrons. Because magnons transfer spin $S^z = -1$ from one electron to another, $\mathcal{H}_{\mathrm{K}}^{xy}$ flips the spin of the electron, whereas $\mathcal{H}_{\mathrm{K}}^{z}$ does not affect spins of conduction electrons. Performing the Fourier transformation, we obtain

$$\mathcal{H}_{\mathrm{K}}^{z0} = \frac{J_{\mathrm{K}}^{\parallel}S}{2}\sum_{\boldsymbol{k}} (c_{\boldsymbol{k}\uparrow}^{\dagger}c_{\boldsymbol{k}\uparrow} - c_{\boldsymbol{k}\downarrow}^{\dagger}c_{\boldsymbol{k}\downarrow}) \tag{2.18}$$

$$\mathcal{H}_{\mathrm{K}}^{xy} = J_{\mathrm{K}}^{\perp}\sqrt{\frac{S}{2N}}\sum_{\boldsymbol{k}\boldsymbol{q}} (a_{\boldsymbol{q}}c_{\boldsymbol{k}+\boldsymbol{q}\downarrow}^{\dagger}c_{\boldsymbol{k}\uparrow} + a_{\boldsymbol{q}}^{\dagger}c_{\boldsymbol{k}\uparrow}^{\dagger}c_{\boldsymbol{k}+\boldsymbol{q}\downarrow}) \tag{2.19}$$

$$\begin{aligned}\mathcal{H}_{\mathrm{K}}^{z} = &-\frac{J_{\mathrm{K}}^{\parallel}}{2N}\sum_{\boldsymbol{q}'\neq\boldsymbol{0}}\sum_{\boldsymbol{k},\boldsymbol{q}} a_{\boldsymbol{q}-\boldsymbol{q}'}^{\dagger}a_{\boldsymbol{q}}(c_{\boldsymbol{k}+\boldsymbol{q}'\uparrow}^{\dagger}c_{\boldsymbol{k}\uparrow} - c_{\boldsymbol{k}+\boldsymbol{q}'\downarrow}^{\dagger}c_{\boldsymbol{k}\downarrow}) \\ &-\frac{J_{\mathrm{K}}^{\parallel}}{2N}\sum_{\boldsymbol{q}} a_{\boldsymbol{q}}^{\dagger}a_{\boldsymbol{q}}\sum_{\boldsymbol{k}}(c_{\boldsymbol{k}\uparrow}^{\dagger}c_{\boldsymbol{k}\uparrow} - c_{\boldsymbol{k}\downarrow}^{\dagger}c_{\boldsymbol{k}\downarrow}).\end{aligned} \tag{2.20}$$

With definitions

$$\mathcal{H}_{\mathrm{K}}^{\parallel 0} = \frac{J_{\mathrm{K}}^{\parallel}\langle S_i^z\rangle}{2}\sum_{\boldsymbol{k}}(c_{\boldsymbol{k}\uparrow}^{\dagger}c_{\boldsymbol{k}\uparrow} - c_{\boldsymbol{k}\downarrow}^{\dagger}c_{\boldsymbol{k}\downarrow}) \tag{2.21}$$

$$\mathcal{H}_{\mathrm{K}}^{\parallel} = -\frac{J_{\mathrm{K}}^{\parallel}}{2N}\sum_{\boldsymbol{k},\boldsymbol{q},\boldsymbol{q}'\neq\boldsymbol{0}} a_{\boldsymbol{q}-\boldsymbol{q}'}^{\dagger}a_{\boldsymbol{q}}(c_{\boldsymbol{k}+\boldsymbol{q}'\uparrow}^{\dagger}c_{\boldsymbol{k}\uparrow} - c_{\boldsymbol{k}+\boldsymbol{q}'\downarrow}^{\dagger}c_{\boldsymbol{k}\downarrow}), \tag{2.22}$$

and $\mathcal{H}_{\mathrm{K}}^{\perp} \equiv \mathcal{H}_{\mathrm{K}}^{xy}$, we obtain $\mathcal{H}_{\mathrm{K}} = \mathcal{H}_{\mathrm{K}}^{\parallel 0} + \mathcal{H}_{\mathrm{K}}^{\parallel} + \mathcal{H}_{\mathrm{K}}^{\perp}$. In order to apply the perturbation theory, we divide the fermion-magnon model into two parts as

$$\mathcal{H} = \mathcal{H}_0 + \mathcal{H}_1, \tag{2.23}$$

where

$$\begin{aligned}\mathcal{H}_0 &= \mathcal{H}_t + \mathcal{H}_{\mathrm{sw}} + \mathcal{H}_{\mathrm{K}}^{\parallel 0} \\ &= \sum_{\boldsymbol{k}}\xi_{\boldsymbol{k}\sigma}c_{\boldsymbol{k}\sigma}^{\dagger}c_{\boldsymbol{k}\sigma} + \sum_{\boldsymbol{q}}\omega_{\boldsymbol{q}}a_{\boldsymbol{q}}^{\dagger}a_{\boldsymbol{q}}\end{aligned} \tag{2.24}$$

and

$$\mathcal{H}_1 = \mathcal{H}_{\mathrm{K}}^{\perp} + \mathcal{H}_{\mathrm{K}}^{\parallel}, \tag{2.25}$$

with

$$\xi_{\boldsymbol{k}\sigma} = \xi_{\boldsymbol{k}}^{(0)} + \sigma h, \tag{2.26}$$

$$h = \frac{1}{2}J_{\mathrm{K}}^{\parallel}\langle S_i^z\rangle, \tag{2.27}$$

$$\omega_{\boldsymbol{q}} = zJ^{\parallel}S[1 - \frac{J^{\perp}}{J^{\parallel}}\gamma(\boldsymbol{q})]. \tag{2.28}$$

Assuming $t_{ij} = -t$ with $t > 0$ for nearest-neighbor sites (i, j), and $t_{ij} = 0$ otherwise, we obtain

$$\xi_{\boldsymbol{k}}^{(0)} = -zt\gamma(\boldsymbol{k}) - \mu. \tag{2.29}$$

We use units in which $t = 1$.

2.2 Pairing susceptibility

The pairing susceptibility χ_{pair} is a convenient tool to find superconducting transition points. χ_{pair} is positive finite in the normal phase, whereas it diverges at the superconducting transition points. This behavior is analogous to that of the magnetic susceptibility χ_{mag} near the magnetic transition point. For example, if we obtain χ_{pair} as a function of the temperature, $\chi_{\mathrm{pair}} \to \infty$ as $T \to T_{\mathrm{c}}$, where T_{c} is the superconducting transition temperature. Below T_{c}, the superconducting order parameter is finite, which implies the spontaneous gauge-symmetry breaking. This is analogous to the fact that below the temperature at which χ_{mag} diverges, the spontaneous magnetization appears. We define the generalized Cooper pair annihilation operator

$$\hat{\psi}_{\sigma\bar{\sigma}}(\boldsymbol{q}, \boldsymbol{k}, \tau_1, \tau) = c_{\boldsymbol{k}+\boldsymbol{q}/2,\sigma}(\tau_1) c_{-\boldsymbol{k}+\boldsymbol{q}/2,\bar{\sigma}}(\tau), \tag{2.30}$$

with

$$A(\tau) = e^{\tau\mathcal{H}} A e^{-\tau\mathcal{H}}, \tag{2.31}$$

where A is an annihilation operator. Using symmetry function γ^α, the Cooper pair annihilation operator can be rewritten as

$$\hat{\psi}^{\alpha}_{\sigma\bar{\sigma}}(\boldsymbol{q}, \tau_1, \tau) = \frac{1}{\sqrt{1+\delta_{\sigma\bar{\sigma}}}} \sum_{\boldsymbol{k}} \gamma^\alpha(\boldsymbol{k}) \hat{\psi}_{\sigma\bar{\sigma}}(\boldsymbol{q}, \boldsymbol{k}, \tau_1, \tau). \tag{2.32}$$

We define even- and odd-frequency Cooper-pair annihilation operators

$$\hat{\psi}^{\alpha(+)}_{\sigma\bar{\sigma}}(\boldsymbol{q}, \tau) = \hat{\psi}^{\alpha}_{\sigma\bar{\sigma}}(\boldsymbol{q}, \tau, \tau), \tag{2.33}$$

$$\hat{\psi}^{\alpha(-)}_{\sigma\bar{\sigma}}(\boldsymbol{q}, \tau) = \left[\frac{\partial}{\partial \tau_1} \hat{\psi}^{\alpha}_{\sigma\bar{\sigma}}(\boldsymbol{q}, \tau_1, \tau)\right]_{\tau_1=\tau}, \tag{2.34}$$

respectively. Superconducting order parameter is written as $\langle\hat{\psi}^{\alpha(\pm)}_{\sigma\bar{\sigma}}(\boldsymbol{q},\tau)\rangle$. In the fermion-magnon model,

$$\begin{aligned}\frac{\partial}{\partial\tau}c_{\boldsymbol{k},\sigma}(\tau) &= [\mathcal{H},c_{\boldsymbol{k},\sigma}(\tau)]\\ &= -\xi_{\boldsymbol{k}\sigma}c_{\boldsymbol{k},\sigma}(\tau)-\sigma\frac{J_{\mathrm{K}}^{\parallel}}{2}\sum_{\boldsymbol{q}'\neq\boldsymbol{0}}S^{z}_{\boldsymbol{q}'}(\tau)c_{\boldsymbol{k}-\boldsymbol{q}',\sigma}(\tau)\\ &\quad -\frac{J_{\mathrm{K}}^{\perp}}{2}\sum_{\boldsymbol{q}'}S^{-\sigma}_{\boldsymbol{q}'}(\tau)c_{\boldsymbol{k}+\sigma\boldsymbol{q}',-\sigma}(\tau).\end{aligned}\tag{2.35}$$

Therefore, the odd-frequency-superconducting order parameter is written as

$$\begin{aligned}\langle\hat{\psi}^{\alpha(-)}_{\sigma\bar{\sigma}}(\boldsymbol{q},\tau)\rangle &= \frac{1}{\sqrt{1+\delta_{\sigma\bar{\sigma}}}}\sum_{\boldsymbol{k}}\gamma^{\alpha}(\boldsymbol{k})\langle\frac{\partial c_{\boldsymbol{k}+\boldsymbol{q}/2,\sigma}(\tau)}{\partial\tau}c_{-\boldsymbol{k}+\boldsymbol{q}/2,\bar{\sigma}}(\tau)\rangle\\ &= \frac{-1}{\sqrt{1+\delta_{\sigma\bar{\sigma}}}}\Big[\sum_{\boldsymbol{k}}\gamma^{\alpha}(\boldsymbol{k})\xi_{\boldsymbol{k}+\frac{\boldsymbol{q}}{2}\sigma}\langle\hat{\psi}^{(+)}_{\sigma\bar{\sigma}}(\boldsymbol{k},\boldsymbol{q},\tau)\rangle\\ &\quad +\sigma\frac{J_{\mathrm{K}}^{\parallel}}{2}\sum_{\boldsymbol{q}'\neq\boldsymbol{0}}\sum_{\boldsymbol{k}}\gamma^{\alpha}(\boldsymbol{k}+\frac{\boldsymbol{q}}{2})\langle S^{z}_{\boldsymbol{q}'}(\tau)\hat{\psi}^{(+)}_{\sigma\bar{\sigma}}(\boldsymbol{k},\boldsymbol{q}-\boldsymbol{q}',\tau)\rangle\\ &\quad +\frac{J_{\mathrm{K}}^{\perp}}{2}\sum_{\boldsymbol{q}'}\sum_{\boldsymbol{k}}\gamma^{\alpha}(\boldsymbol{k}-\sigma\frac{\boldsymbol{q}}{2})\langle S^{-\sigma}_{\boldsymbol{q}'}(\tau)\hat{\psi}^{(+)}_{-\sigma\bar{\sigma}}(\boldsymbol{k},\boldsymbol{q}+\sigma\boldsymbol{q}',\tau)\rangle\Big].\end{aligned}\tag{2.36}$$

Thus, we find that odd-frequency superconductivity can be taken as composite order. We define the pairing susceptibility

$$\chi^{\alpha(\pm)}_{\sigma\bar{\sigma}}(\boldsymbol{q},\tau-\tau')=\frac{1}{N}\langle T_{\tau}[\hat{\psi}^{\alpha(\pm)}_{\sigma\bar{\sigma}}(\boldsymbol{q},\tau)\hat{\psi}^{\alpha(\pm)\dagger}_{\sigma\bar{\sigma}}(\boldsymbol{q},\tau')]\rangle.\tag{2.37}$$

When $\chi^{\alpha(\pm)}_{\sigma\bar{\sigma}}(\boldsymbol{q})$ diverges, the order parameter $\langle\hat{\psi}^{\alpha(\pm)}_{\sigma\bar{\sigma}}(\boldsymbol{q})\rangle$ begins to have a finite value, and thus the superconducting transition occurs. In the interaction picture,

$$\chi^{\alpha(\pm)}_{\sigma\bar{\sigma}}(\boldsymbol{q},\tau-\tau')=\frac{1}{N}\frac{\langle T_{\tau}[U_I(\beta)\hat{\psi}^{\alpha(\pm)}_{I\sigma\bar{\sigma}}(\boldsymbol{q},\tau)\hat{\psi}^{\alpha(\pm)\dagger}_{I\sigma\bar{\sigma}}(\boldsymbol{q},\tau')]\rangle_0}{\langle U_I(\beta)\rangle_0},\tag{2.38}$$

where

$$A_I(\tau)=e^{\tau\mathcal{H}_0}\,A\,e^{-\tau\mathcal{H}_0},\tag{2.39}$$

$$U_I(\tau)=U_0^{\dagger}(\tau)U(\tau)=\int_0^{\tau}d\tau' T_{\tau}[e^{-\mathcal{H}_{1I}(\tau')\tau'}],\tag{2.40}$$

$$\langle \cdots \rangle_0 \equiv \mathrm{Tr}[\rho_0 \cdots], \tag{2.41}$$

$$\rho_0 = \frac{e^{-\tau \mathcal{H}_0}}{\mathrm{Tr}[e^{-\tau \mathcal{H}_0}]}. \tag{2.42}$$

Therefore, unperturbed pairing susceptibilities are

$$\chi^{\alpha(\pm)}_{0\sigma\bar{\sigma}}(\boldsymbol{q}, \tau - \tau') = \frac{1}{N} \langle T_\tau [\hat{\psi}^{\alpha(\pm)}_{I\sigma\bar{\sigma}}(\boldsymbol{q}, \tau) \hat{\psi}^{\alpha(\pm)\dagger}_{I\sigma\bar{\sigma}}(\boldsymbol{q}, \tau')] \rangle_0, \tag{2.43}$$

$$\begin{aligned} \chi^{\alpha(+)}_{0\sigma\bar{\sigma}}(\boldsymbol{q}, \tau - \tau') = \frac{1}{N} \frac{1}{1+\delta_{\sigma\bar{\sigma}}} \sum_{\boldsymbol{k},\boldsymbol{k}'} \gamma^\alpha(\boldsymbol{k}) \gamma^{\alpha *}(\boldsymbol{k}') (\delta_{\boldsymbol{k}\boldsymbol{k}'} - \delta_{\sigma\bar{\sigma}} \delta_{-\boldsymbol{k}\boldsymbol{k}'}) \\ \times G_{0\sigma}(\boldsymbol{k} + \frac{\boldsymbol{q}}{2}, \tau - \tau') G_{0\bar{\sigma}}(-\boldsymbol{k} + \frac{\boldsymbol{q}}{2}, \tau - \tau'), \end{aligned} \tag{2.44}$$

$$\begin{aligned} \chi^{\alpha(-)}_{0\sigma\bar{\sigma}}(\boldsymbol{q}, \tau - \tau') = \frac{1}{N} \frac{1}{1+\delta_{\sigma\bar{\sigma}}} \sum_{\boldsymbol{k},\boldsymbol{k}'} \gamma^\alpha(\boldsymbol{k}) \gamma^{\alpha *}(\boldsymbol{k}') \\ \times \Big(\delta_{\boldsymbol{k}\boldsymbol{k}'} \Big[\frac{\partial}{\partial \tau} \frac{\partial}{\partial \tau'} G_{0\sigma}(\boldsymbol{k} + \frac{\boldsymbol{q}}{2}, \tau - \tau') \Big] G_{0\bar{\sigma}}(-\boldsymbol{k} + \frac{\boldsymbol{q}}{2}, \tau - \tau') \\ - \delta_{\sigma\bar{\sigma}}\, \delta_{-\boldsymbol{k}\boldsymbol{k}'} \Big[\frac{\partial}{\partial \tau} G_{0\sigma}(\boldsymbol{k} + \frac{\boldsymbol{q}}{2}, \tau - \tau') \Big] \Big[\frac{\partial}{\partial \tau'} G_{0\bar{\sigma}}(-\boldsymbol{k} + \frac{\boldsymbol{q}}{2}, \tau - \tau') \Big] \Big), \end{aligned} \tag{2.45}$$

with

$$G_{0\sigma}(\boldsymbol{k}, \tau - \tau') = -\langle T_\tau [c_{I\boldsymbol{k},\sigma}(\tau) c^\dagger_{I\boldsymbol{k},\sigma}(\tau')] \rangle_0. \tag{2.46}$$

The Fourier transform of the susceptibility and the Green's function are defined

$$\chi^{\alpha(\pm)}_{\sigma\bar{\sigma}}(\boldsymbol{q}, i\nu_m) = \int_0^\beta \chi^{\alpha(\pm)}_{\sigma\bar{\sigma}}(\boldsymbol{q}, \tau) e^{i\nu_m \tau} d\tau, \tag{2.47}$$

$$G_\sigma(\boldsymbol{k}, i\omega_n) = \int_0^\beta G_\sigma(\boldsymbol{k}, \tau) e^{i\omega_n \tau} d\tau, \tag{2.48}$$

respectively, where

$$\nu_m = \frac{\pi}{\beta} 2m, \tag{2.49}$$

$$\omega_n = \frac{\pi}{\beta}(2n+1), \tag{2.50}$$

with integers m and n. We define $q = (\boldsymbol{q}, i\nu_m)$ and $k = (\boldsymbol{k}, i\omega_n)$. The Fourier transforms of unperturbed pairing susceptibilities are

$$\chi^{\alpha(+)}_{0\sigma\bar{\sigma}}(q) = \frac{T}{N}\sum_{k,k'}\gamma^{\alpha}(\boldsymbol{k})\gamma^{\alpha*}(\boldsymbol{k}')\delta_{n+n',m}\frac{\delta_{\boldsymbol{k}\boldsymbol{k}'} - \delta_{\sigma\bar{\sigma}}\delta_{-\boldsymbol{k}\boldsymbol{k}'}}{1+\delta_{\sigma\bar{\sigma}}} \times G_{0\sigma}(\boldsymbol{k}+\frac{\boldsymbol{q}}{2}, i\omega_n)G_{0\bar{\sigma}}(-\boldsymbol{k}+\frac{\boldsymbol{q}}{2}, i\omega_{n'}), \tag{2.51}$$

$$\chi^{\alpha(-)}_{0\sigma\bar{\sigma}}(q) = \frac{T}{N}\sum_{k,k'}\gamma^{\alpha}(\boldsymbol{k})\gamma^{\alpha*}(\boldsymbol{k}')\delta_{n+n',m}\frac{\omega_n\omega_n\delta_{\boldsymbol{k}\boldsymbol{k}'} - \omega_n\omega_{n'}\delta_{\sigma\bar{\sigma}}\delta_{-\boldsymbol{k}\boldsymbol{k}'}}{1+\delta_{\sigma\bar{\sigma}}} \times G_{0\sigma}(\boldsymbol{k}+\frac{\boldsymbol{q}}{2}, i\omega_n)G_{0\bar{\sigma}}(-\boldsymbol{k}+\frac{\boldsymbol{q}}{2}, i\omega_{n'}). \tag{2.52}$$

In particular, when $q = 0$,

$$\chi^{\alpha(\pm)}_{0\sigma\bar{\sigma}}(0) = \frac{T}{N}\sum_{k}\frac{\gamma^{\alpha}_{(\pm)}(k)\gamma^{\alpha*}_{(\pm)}(k) - \delta_{\sigma\bar{\sigma}}\gamma^{\alpha}_{(\pm)}(k)\gamma^{\alpha*}_{(\pm)}(-k)}{1+\delta_{\sigma\bar{\sigma}}}w_{\sigma\bar{\sigma}}(k), \tag{2.53}$$

with

$$\gamma^{\alpha}_{(+)}(k) = \gamma^{\alpha}(\boldsymbol{k}), \tag{2.54}$$

$$\gamma^{\alpha}_{(-)}(k) = \omega_n\gamma^{\alpha}(\boldsymbol{k}), \tag{2.55}$$

$$w_{\sigma\bar{\sigma}}(k) = G_{0\sigma}(k)G_{0\bar{\sigma}}(-k). \tag{2.56}$$

We obtain a simpler expression

$$\chi^{\alpha(\pm)}_{0\sigma\bar{\sigma}}(0) = \frac{T}{N}\sum_{k}|\gamma^{\alpha}_{(\pm)}(k)|^2 w_{\sigma\bar{\sigma}}(k), \tag{2.57}$$

if we assume that, when $\sigma = \bar{\sigma}$, the symmetry must be either even-frequency odd-parity or odd-frequency even-parity. Hereafter, we examine the pairing susceptibility with $q = 0$, because in most situations the superconducting state is energetically stable at $q = 0$. In particular, for $\bar{\sigma} = \sigma$, the pairing susceptibility is the largest at $q = 0$ independently of the value of h, because $\sigma h = \bar{\sigma}h$ only shifts the chemical potential. For $\bar{\sigma} \neq \sigma$, the pairing susceptibility is the largest at $q = 0$ when $h = 0$, whereas when $h \neq 0$, it can be largest at $q \neq 0$. The superconducting state due to Cooper pairs of two electrons with antiparallel spin and $\boldsymbol{q} \neq 0$ can be stable, when h is on the order of the superconductive energy gap Δ_0. Such a state is called the Fulde-Ferrell-Larkin-Ovchinnicov state [40, 41].

2.3 Magnon exchange interactions

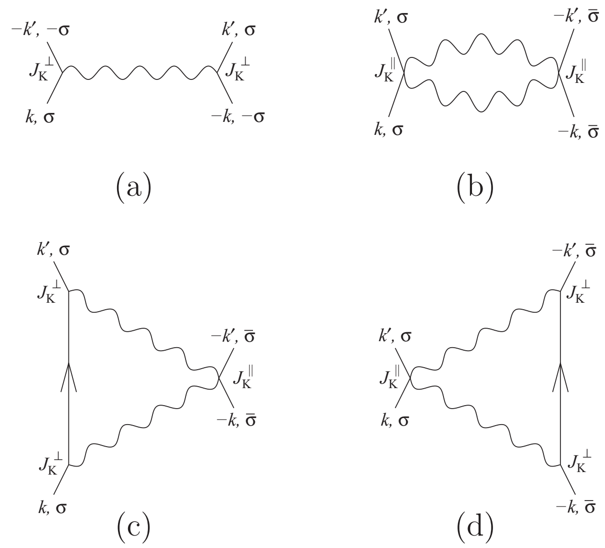

Fig 2.1: Feynman diagrams that represent effective interactions. The solid and wavy lines are the electron and magnon Green's functions, respectively [42].

In this section, we derive the effective interactions by the perturbation theory. In the fermion-magnon system, magnons can mediate the interactions between electrons. We consider the second order term and the third order term of the electron-magnon interaction $\mathcal{H}_1$ in the ferromagnetic-metal state. We examine the interactions shown in Fig. 2.1. The first-order term does not exist. The second order terms are

$$\begin{aligned}\Gamma^{(1)}_{\sigma,-\sigma} &= \frac{1}{2} {J_{\mathrm{K}}^{\perp}}^2 S D(-\sigma(k+k')) \\ &= \frac{1}{2} {J_{\mathrm{K}}^{\perp}}^2 S \frac{1}{-i\sigma\nu_{n+n'} + \omega_{\boldsymbol{k}+\boldsymbol{k}'}},\end{aligned} \tag{2.58}$$

which are expressed in Fig. 2.1(a), and

$$\begin{aligned}\Gamma^{(2)}_{\sigma\bar{\sigma}} &= \sigma\bar{\sigma}\frac{{J_{\mathrm{K}}^{\parallel}}^2}{4}\frac{T}{N}\sum_{k_1} D(k_1-k')D(k_1-k) \\ &= -\sigma\bar{\sigma}\frac{{J_{\mathrm{K}}^{\parallel}}^2}{4}\frac{1}{N}\sum_{\boldsymbol{k}_1}[n(\omega_{\boldsymbol{k}_1-\boldsymbol{k}'}) - n(\omega_{\boldsymbol{k}_1-\boldsymbol{k}})]\frac{\omega_{\boldsymbol{k}_1-\boldsymbol{k}'} - \omega_{\boldsymbol{k}_1-\boldsymbol{k}}}{\nu^2_{n'-n} + (\omega_{\boldsymbol{k}_1-\boldsymbol{k}'} - \omega_{\boldsymbol{k}_1-\boldsymbol{k}})^2},\end{aligned} \tag{2.59}$$

which are expressed in Fig. 2.1(b). Here, $n(\omega_{\boldsymbol{q}})$ is the Bose distribution function of magnons. The interaction $\Gamma^{(1)}_{\sigma,-\bar{\sigma}}$ is induced by one-magnon-exchange. This process is of the second order of $\mathcal{H}_{\mathrm{K}}^{\perp}$. This interaction is analogous to the phonon-mediated interaction. However, differently from that mediated by phonons $\Gamma^{(1)}_{\sigma,-\sigma}$ depends on the electron spin. As a result, $\Gamma^{(1)}_{\sigma,-\sigma}$ contributes to only antiparallel spin pairing. The interaction $\Gamma^{(2)}_{\sigma\bar{\sigma}}$ is induced by two-magnon-exchange. This interaction is of the second order of $\mathcal{H}_{\mathrm{K}}^{\parallel}$, and contributes to both antiparallel and parallel spin pairings, but the sign of the coupling constant is opposite. When $T \to 0$, the two-magnon-exchange interaction $\Gamma^{(2)}_{\sigma\bar{\sigma}} \to 0$, since $n(\omega_{\boldsymbol{q}}) \to 0$. In this feature, the magnon-exchange-interaction contrasts with that in the antiferromagnetic case. Because $\Gamma^{(2)}_{\sigma\bar{\sigma}} \to 0$ when $T \to 0$, we consider the third order terms depicted as triangle processes in Fig. 2.1(c) and Fig. 2.1(d). These terms are expressed as

$$
\begin{aligned}
\Gamma^{(3)}_{\sigma\bar{\sigma}} = & -\frac{J_{\mathrm{K}}^{\parallel} {J_{\mathrm{K}}^{\perp}}^2 S}{4}\frac{T}{N}\sum_{k_1}\Big[\bar{\sigma}G_{-\sigma}(k_1)D(\sigma(k_1-k))D(\sigma(k_1-k')) \\
& \qquad\qquad +\sigma G_{-\bar{\sigma}}(-k_1)D(\bar{\sigma}(k-k_1))D(\bar{\sigma}(k'-k_1))\Big] \\
= & -\sigma\bar{\sigma}\frac{J_{\mathrm{K}}^{\parallel} {J_{\mathrm{K}}^{\perp}}^2 S}{4}\frac{1}{N} \\
& \times\sum_{\boldsymbol{k}_1}\Big[\; f(\sigma\xi_{\boldsymbol{k}_1-\sigma})\frac{1}{i\sigma\omega_n-\sigma\xi_{\boldsymbol{k}_1-\sigma}+\omega_{\boldsymbol{k}_1-\boldsymbol{k}}}\frac{1}{i\sigma\omega_{n'}-\sigma\xi_{\boldsymbol{k}_1-\sigma}+\omega_{\boldsymbol{k}_1-\boldsymbol{k}'}} \\
& \qquad +n(\omega_{\boldsymbol{k}_1-\boldsymbol{k}})\frac{1}{i\sigma\omega_n-\sigma\xi_{\boldsymbol{k}_1-\sigma}+\omega_{\boldsymbol{k}_1-\boldsymbol{k}}}\frac{1}{i\sigma\nu_{n'-n}+\omega_{\boldsymbol{k}_1-\boldsymbol{k}'}-\omega_{\boldsymbol{k}_1-\boldsymbol{k}}} \\
& \qquad -n(\omega_{\boldsymbol{k}_1-\boldsymbol{k}'})\frac{1}{i\sigma\omega_{n'}-\sigma\xi_{\boldsymbol{k}_1-\sigma}+\omega_{\boldsymbol{k}_1-\boldsymbol{k}'}}\frac{1}{i\sigma\nu_{n'-n}+\omega_{\boldsymbol{k}_1-\boldsymbol{k}'}-\omega_{\boldsymbol{k}_1-\boldsymbol{k}}} \\
& \qquad +f(\bar{\sigma}\xi_{\boldsymbol{k}_1-\bar{\sigma}})\frac{1}{-i\bar{\sigma}\omega_n-\bar{\sigma}\xi_{\boldsymbol{k}_1-\bar{\sigma}}+\omega_{\boldsymbol{k}_1-\boldsymbol{k}}}\frac{1}{-i\bar{\sigma}\omega_{n'}-\bar{\sigma}\xi_{\boldsymbol{k}_1-\bar{\sigma}}+\omega_{\boldsymbol{k}_1-\boldsymbol{k}'}} \\
& \qquad +n(\omega_{\boldsymbol{k}_1-\boldsymbol{k}})\frac{1}{-i\bar{\sigma}\omega_n-\bar{\sigma}\xi_{\boldsymbol{k}_1-\bar{\sigma}}+\omega_{\boldsymbol{k}_1-\boldsymbol{k}}}\frac{1}{-i\bar{\sigma}\nu_{n'-n}+\omega_{\boldsymbol{k}_1-\boldsymbol{k}'}-\omega_{\boldsymbol{k}_1-\boldsymbol{k}}} \\
& \qquad -n(\omega_{\boldsymbol{k}_1-\boldsymbol{k}'})\frac{1}{-i\bar{\sigma}\omega_{n'}-\bar{\sigma}\xi_{\boldsymbol{k}_1-\bar{\sigma}}+\omega_{\boldsymbol{k}_1-\boldsymbol{k}'}}\frac{1}{-i\bar{\sigma}\nu_{n'-n}+\omega_{\boldsymbol{k}_1-\boldsymbol{k}'}-\omega_{\boldsymbol{k}_1-\boldsymbol{k}}}\Big],
\end{aligned}
\tag{2.60}
$$

where $f(\xi_{\boldsymbol{k}\sigma})$ is the Fermi distribution function of electrons. Because this equation has terms which are not proportional to $n(\omega_{\boldsymbol{q}})$, $\Gamma^{(3)}_{\sigma\bar{\sigma}}$ survives in the low temperature limit. This interaction contributes both antiparallel and parallel spin pairings. In particular when $\sigma = \bar{\sigma}$, we obtain

$$
\begin{aligned}
\Gamma^{(3)}_{\sigma\sigma} = -\frac{J_{\rm K}^{\parallel} {J_{\rm K}^{\perp}}^2 S}{2} \frac{1}{N} \\
\times \sum_{\boldsymbol{k}_1} \Big[\; & f(\sigma\xi_{\boldsymbol{k}_1-\sigma}) \frac{(\sigma\xi_{\boldsymbol{k}_1-\sigma} - \omega_{\boldsymbol{k}_1-\boldsymbol{k}})(\sigma\xi_{\boldsymbol{k}_1-\sigma} - \omega_{\boldsymbol{k}_1-\boldsymbol{k}'}) - \omega_n\omega_{n'}}{[\omega_n^2 + (\sigma\xi_{\boldsymbol{k}_1-\sigma} - \omega_{\boldsymbol{k}_1-\boldsymbol{k}})^2][\omega_{n'}^2 + (\sigma\xi_{\boldsymbol{k}_1-\sigma} - \omega_{\boldsymbol{k}_1-\boldsymbol{k}'})^2]} \\
& -n(\omega_{\boldsymbol{k}_1-\boldsymbol{k}}) \frac{(\sigma\xi_{\boldsymbol{k}_1-\sigma} - \omega_{\boldsymbol{k}_1-\boldsymbol{k}})(\omega_{\boldsymbol{k}_1-\boldsymbol{k}'} - \omega_{\boldsymbol{k}_1-\boldsymbol{k}}) + \omega_n\nu_{n'-n}}{[\omega_n^2 + (\sigma\xi_{\boldsymbol{k}_1-\sigma} - \omega_{\boldsymbol{k}_1-\boldsymbol{k}})^2][\nu_{n'-n}^2 + (\omega_{\boldsymbol{k}_1-\boldsymbol{k}'} - \omega_{\boldsymbol{k}_1-\boldsymbol{k}})^2]} \\
& +n(\omega_{\boldsymbol{k}_1-\boldsymbol{k}'}) \frac{(\sigma\xi_{\boldsymbol{k}_1-\sigma} - \omega_{\boldsymbol{k}_1-\boldsymbol{k}'})(\omega_{\boldsymbol{k}_1-\boldsymbol{k}'} - \omega_{\boldsymbol{k}_1-\boldsymbol{k}}) + \omega_{n'}\nu_{n'-n}}{[\omega_{n'}^2 + (\sigma\xi_{\boldsymbol{k}_1-\sigma} - \omega_{\boldsymbol{k}_1-\boldsymbol{k}'})^2][\nu_{n'-n}^2 + (\omega_{\boldsymbol{k}_1-\boldsymbol{k}'} - \omega_{\boldsymbol{k}_1-\boldsymbol{k}})^2]} \Big].
\end{aligned}
\tag{2.61}
$$

Thus, $\Gamma^{(3)}_{\sigma\bar{\sigma}}$ is the lowest order effective interaction that contributes to parallel spin pairing in the limit $T \to 0$. Hereafter, we examine only parallel spin pairing, because antiparallel spin pairing is suppressed by the strong exchange field. Therefore, we omit $\Gamma^{(1)}_{\sigma,-\sigma}$ and examine $\Gamma^{(2)}_{\sigma\sigma}$ and $\Gamma^{(3)}_{\sigma\sigma}$. From Eqs. (2.59) and (2.61), we find that $\Gamma^{(2)}_{\sigma\sigma}$ and $\Gamma^{(3)}_{\sigma\sigma}$ are invariant under simultaneous reversing signs of ω_n and $\omega_{n'}$. Therefore, $\Gamma^{(2)}_{\sigma\sigma}$ and $\Gamma^{(3)}_{\sigma\sigma}$ can be divided into even-frequency and odd-frequency parts defined by

$$
\begin{aligned}
\Gamma^{(\pm)}_{\sigma\sigma}(\boldsymbol{k}, i\omega_n, \boldsymbol{k}', i\omega_{n'}) &= \pm\Gamma^{(\pm)}_{\sigma\sigma}(\boldsymbol{k}, -i\omega_n, \boldsymbol{k}', i\omega_{n'}) \\
&= \pm\Gamma^{(\pm)}_{\sigma\sigma}(\boldsymbol{k}, i\omega_n, \boldsymbol{k}', -i\omega_{n'}).
\end{aligned}
\tag{2.62}
$$

In a similar way, $\Gamma^{(2)}_{\sigma\sigma}$ and $\Gamma^{(3)}_{\sigma\sigma}$ can also be divided into even-parity and odd-parity parts defined by

$$
\begin{aligned}
\Gamma^{e}_{\sigma\sigma}(\boldsymbol{k}, i\omega_n, \boldsymbol{k}', i\omega_{n'}) &= +\Gamma^{e}_{\sigma\sigma}(-\boldsymbol{k}, i\omega_n, \boldsymbol{k}', i\omega_{n'}) \\
&= +\Gamma^{e}_{\sigma\sigma}(\boldsymbol{k}, i\omega_n, -\boldsymbol{k}', i\omega_{n'}),
\end{aligned}
\tag{2.63}
$$

and

$$
\begin{aligned}
\Gamma^{o}_{\sigma\sigma}(\boldsymbol{k}, i\omega_n, \boldsymbol{k}', i\omega_{n'}) &= -\Gamma^{o}_{\sigma\sigma}(-\boldsymbol{k}, i\omega_n, \boldsymbol{k}', i\omega_{n'}) \\
&= -\Gamma^{o}_{\sigma\sigma}(\boldsymbol{k}, i\omega_n, -\boldsymbol{k}', i\omega_{n'}).
\end{aligned}
\tag{2.64}
$$

2.4 Phase transitions

The pairing susceptibilities $\chi^{\alpha(\pm)}_{\sigma\sigma}$ can be expressed as

$$\chi^{\alpha(\pm)}_{\sigma\sigma} = \chi^{\alpha(\pm)}_{0\sigma\sigma} + \frac{T^2}{N^2}\sum_{k,k'}\gamma^{\alpha}_{(\pm)}(k)w_{\sigma\sigma}(k)\Gamma^{\rm red}_{\sigma\sigma}(k,k')w_{\sigma\sigma}(k')\gamma^{\alpha*}_{(\pm)}(k'), \tag{2.65}$$

where $\Gamma^{\rm red}_{\sigma\sigma}(k,k')$ is the reducible vertex part. In the present study, we neglect self-energies of the electron and the magnon for simplicity. Equation (2.65) is expressed in matrix form

$$\chi^{\alpha(\pm)}_{\sigma\sigma} = \hat{\gamma}^{\alpha(\pm)}_{\sigma\sigma}\hat{W}_{\sigma\sigma}\hat{\gamma}^{\alpha(\pm)\dagger}_{\sigma\sigma} + \hat{\gamma}^{\alpha(\pm)}_{\sigma\sigma}\hat{W}_{\sigma\sigma}\hat{\Gamma}^{\rm red}_{\sigma\sigma}\hat{W}_{\sigma\sigma}\hat{\gamma}^{\alpha(\pm)\dagger}_{\sigma\sigma}. \tag{2.66}$$

Here, $\hat{W}_{\sigma\sigma}$ and $\hat{\Gamma}^{\rm red}_{\sigma\sigma}$ are matrices whose elements are $\delta_{kk'}(T/N)w_{\sigma\sigma}(k)$ and $\Gamma^{\rm red}_{\sigma\sigma}(k,k')$, respectively. $\hat{\gamma}^{\alpha(\pm)}_{\sigma\sigma}$ is the row vector whose elements are $\gamma^{\alpha}_{(\pm)}(k)$. We define the irreducible vertex part $\hat{\Gamma}_{\sigma\sigma}$ by

$$\hat{\Gamma}^{\rm red}_{\sigma\sigma} = \hat{\Gamma}_{\sigma\sigma} + \hat{\Gamma}^{\rm red}_{\sigma\sigma}\hat{W}_{\sigma\sigma}\hat{\Gamma}_{\sigma\sigma} = [\mathbf{1} - \hat{\Gamma}_{\sigma\sigma}\hat{W}_{\sigma\sigma}]^{-1}\hat{\Gamma}_{\sigma\sigma}. \tag{2.67}$$

Thus, we obtain

$$\begin{aligned}\chi^{\alpha(\pm)}_{\sigma\sigma} &= \hat{\gamma}^{\alpha(\pm)}_{\sigma\sigma}\hat{W}_{\sigma\sigma}\hat{\Gamma}^{\rm red}_{\sigma\sigma}\hat{\Gamma}^{-1}_{\sigma\sigma}\hat{\gamma}^{\alpha(\pm)\dagger}_{\sigma\sigma} \\ &= \hat{\gamma}^{\alpha(\pm)}_{\sigma\sigma}\hat{W}_{\sigma\sigma}[\mathbf{1} - \hat{\Gamma}_{\sigma\sigma}\hat{W}_{\sigma\sigma}]^{-1}\hat{\gamma}^{\alpha(\pm)\dagger}_{\sigma\sigma} \\ &= \hat{\gamma}^{\alpha(\pm)}_{\sigma\sigma}[\hat{W}^{-1}_{\sigma\sigma} - \hat{\Gamma}_{\sigma\sigma}]^{-1}\hat{\gamma}^{\alpha(\pm)\dagger}_{\sigma\sigma},\end{aligned} \tag{2.68}$$

where $\mathbf{1}$ is the identity matrix, and

$$\chi^{\alpha(\pm)}_{\sigma\sigma} = \hat{v}^{\alpha(\pm)}_{\sigma\sigma}[\mathbf{1} - \hat{\Lambda}_{\sigma\sigma}]^{-1}\hat{v}^{\alpha(\pm)\dagger}_{\sigma\sigma}, \tag{2.69}$$

with

$$\hat{v}^{\alpha(\pm)}_{\sigma\sigma} = \hat{\gamma}^{\alpha(\pm)}_{\sigma\sigma}\hat{W}^{1/2}_{\sigma\sigma}, \tag{2.70}$$

$$\hat{\Lambda}_{\sigma\sigma} = \hat{W}^{1/2}_{\sigma\sigma}\hat{\Gamma}_{\sigma\sigma}\hat{W}^{1/2}_{\sigma\sigma}. \tag{2.71}$$

Divergence of the pairing susceptibilities $\chi^{\alpha(\pm)}_{\sigma\sigma}$ indicates instability of the normal state. Therefore, with varying a parameter such as the temperature in the normal state, at the parameter value, where $\chi^{\alpha(\pm)}_{\sigma\sigma}$ diverges for the first time, the phase transition occurs from normal state to the superconducting state. In order to find a superconducting transition temperature and the pairing symmetry, we consider the eigenequation

$$\hat{\Lambda}_{\sigma\sigma}\hat{v} = \lambda\hat{v}, \tag{2.72}$$

where λ and $\hat{v}$ are the largest eigenvalue of $\hat{\Lambda}_{\sigma\sigma}$ and the corresponding eigenvector, respectively. When $\lambda < 1$, $\chi^{\alpha(\pm)}_{\sigma\sigma}$ is finite and positive for any $\hat{\gamma}^{\alpha(\pm)}_{\sigma\sigma}$, which implies that the normal state is stable. When $\lambda \to 1$ and $\hat{\gamma}^{\alpha(\pm)}_{\sigma\sigma}$ has a component proportional to $\hat{v}$, $\chi^{\alpha(\pm)}_{\sigma\sigma}$ diverges as $\chi^{\alpha(\pm)}_{\sigma\sigma} \sim (1-\lambda)^{-1} \to \infty$, and the phase transition occurs. Therefore, the superconducting transition temperature is obtained by the condition $\lambda = 1$. The corresponding eigenvector $\hat{v}$ reflects the pairing symmetry just below the superconducting transition temperature.

Chapter 3

Results

We numerically solve the eigenequation (2.72). As an illustration, we examine a quasi-one-dimensional system. This simplification in the model significantly reduces numerical task for solving the eigenequation, which is quite heavy in general, and allows us to fully account for the spatial and temporal dependences. Accurate treatment of these dependences is significant in examination of odd-frequency superconductivity. However, in order to stabilize the long-range order at finite temperatures, interchain coupling ($t' \gg T$) is assumed. At the same time, we assume $t \gg t'$, and omit the small interchain coupling in the following equations. These assumptions can be consistent when $t \gg T$. Thus, we obtain

$$\xi_{\boldsymbol{k}\sigma} = -2t\cos k_x - \mu + \sigma \frac{J_{\mathrm{K}}^{\parallel}\langle S_i^z \rangle}{2}, \tag{3.1}$$

$$\omega_{\boldsymbol{q}} = J^{\parallel}(1 - \frac{J^{\perp}}{J^{\parallel}}\cos q_x), \tag{3.2}$$

where $S = 1/2$. The number of electrons per site n_{e} is obtained by

$$n_{\mathrm{e}} = \frac{1}{N}\sum_{\boldsymbol{k},\sigma} f(\xi_{\boldsymbol{k}\sigma}). \tag{3.3}$$

We examine the pairing susceptibility for parallel spin pairing with zero center of mass momentum as mentioned above. We call the superconducting state of even-frequency odd-parity $\sigma\sigma$-spin pairing the EO$\sigma\sigma$ state and that of odd-frequency even-parity $\sigma\sigma$-spin pairing the OE$\sigma\sigma$ state hereafter, where $\sigma = \uparrow$ or $\downarrow$. When $n_{\mathrm{e}} = 1$, the pairing susceptibility for up-up spin pairing is identical to that for down-down spin pairing, because of the particle-hole symmetry of the system. Therefore, the EO$\uparrow\uparrow$ and EO$\downarrow\downarrow$ states are collectively called the EOT state, and also the OE$\uparrow\uparrow$ and OE$\downarrow\downarrow$ states are collectively called the OET state. We summarize these abbreviations for the superconducting states in Table 3.1.

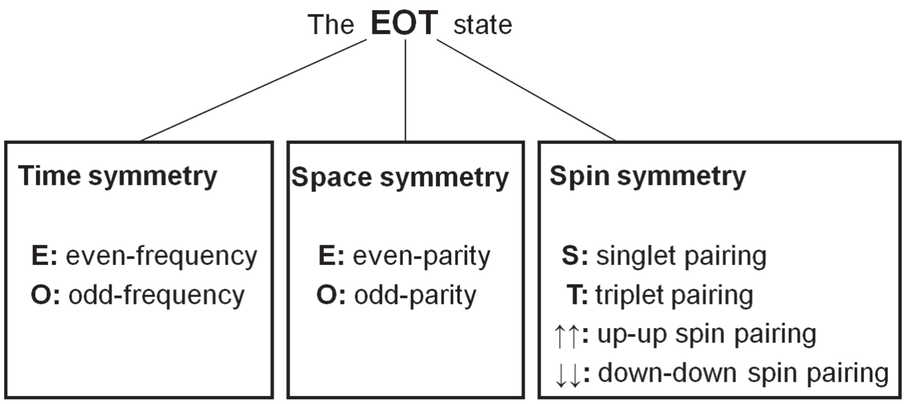

Table 3.1: Definitions of the abbreviations for the superconducting states.

We use units in which $t = 1$. We show the results for $J^{\parallel} = 0.01$, $J^{\perp} = 0.95J^{\parallel}$, and $n_{\mathrm{e}} = 1$ in Secs. 3.1–3.4. For these parameters, the ferromagnetic transition temperature is obtained as $T_{\mathrm{FM}} \approx 2.39 \times 10^{-3}$, from the condition

$$\langle S_i^z \rangle = S - \frac{1}{N} \sum_{\boldsymbol{q}} n(\omega_{\boldsymbol{q}}) = 0. \tag{3.4}$$

In Sec. 3.5, we show the results when $J^{\perp}$ is varied. In Sec. 3.7, we examine n_{e} dependence.

3.1 Temperature dependence of the pairing susceptibility

Figure 3.1 shows $1 - \lambda$ as a function of temperature T for the isotropic Kondo coupling $J_{\mathrm{K}} \equiv J_{\mathrm{K}}^{\parallel} = J_{\mathrm{K}}^{\perp}$. Because $\chi_{\sigma\sigma}^{\alpha(\pm)} \propto (1 - \lambda)^{-1}$, minimum eigenvalue $1 - \lambda$

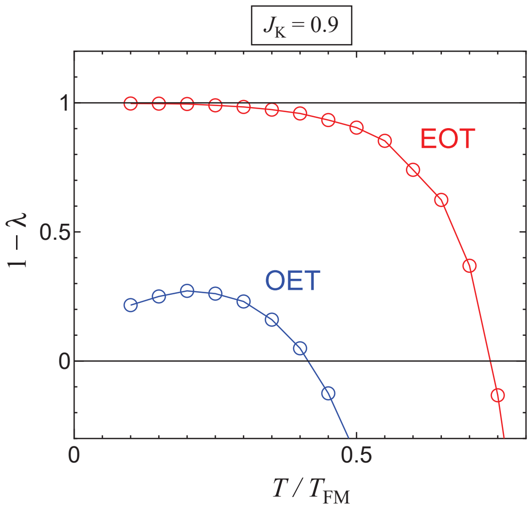

(a)

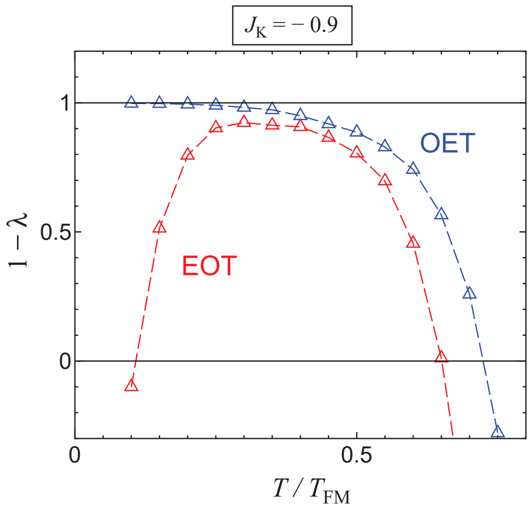

(b)

Fig 3.1: Minimum eigenvalue $1 - \lambda$ as a function of temperature T. We assume the isotropic Kondo coupling $J_K = J_K^{\parallel} = J_K^{\perp}$. The red and blue curves show the results for EOT and OET states, respectively. In panel (a), the open circle and solid curve show the result for $J_K = 0.9$, whereas in panel (b), the open triangle and dashed curve show the result for $J_K = -0.9$. Similar results have been presented in Ref. [42].

gives maximum $\chi_{\sigma\sigma}^{\alpha(\pm)}$. Thus, the phase transition occurs where the curve crosses the line $1-\lambda=0$. Where $1-\lambda>0$, normal state is stable against pairing fluctuations. The perturbation theory breaks down in the region where $1-\lambda<0$.

In Fig. 3.1 (a) for $J_{\mathrm{K}}=0.9$, $1-\lambda$ for the OET state is smallest at any temperature. The normal state is stable in the region $T \lesssim 0.4T_{\mathrm{FM}}$. Transition temperature to the OET state is $T_{\mathrm{c}} \approx 0.4T_{\mathrm{FM}}$. In Fig. 3.1 (b) for $J_{\mathrm{K}}=-0.9$, $1-\lambda$ for the EOT state is smallest at any temperature. In the region $0.1T_{\mathrm{FM}} \lesssim T \lesssim 0.65T_{\mathrm{FM}}$, the normal state is stable, whereas the EOT state occurs in the regions for $T \lesssim 0.1T_{\mathrm{FM}}$ and $T \gtrsim 0.65T_{\mathrm{FM}}$ The unusual reentrant superconducting transition occurs both for $J_{\mathrm{K}}=0.9$ and for $J_{\mathrm{K}}=-0.9$. In Sec. 3.3.2, we show that the normal regions below T_{c} are connected to the normal region near $T=T_{\mathrm{FM}}$ through the normal region around $J_{\mathrm{K}}=0$.

3.2 Spatial and temporal structures of the order parameter

Figure 3.2 shows profiles of eigenvectors at the superconducting transition temperature $T_{\mathrm{c}}=0.8T_{\mathrm{FM}}$. The Kondo coupling is assumed to be isotropic: $J_{\mathrm{K}}=J_{\mathrm{K}}^{\parallel}=J_{\mathrm{K}}^{\perp}$. In Fig. 3.2 (a), $\Delta_{\downarrow\downarrow}(k_x)$ is defined as

$$\Delta_{\downarrow\downarrow}(k_x)=\frac{v(k_x)}{\sqrt{w_{\downarrow\downarrow}(k_x)}}, \tag{3.5}$$

where $v(k_x)$ is the eigenvector of $\Lambda_{\downarrow\downarrow}$. In Fig. 3.2 (b), $\Delta_{\uparrow\uparrow}(k_x)$ is defined as

$$\Delta_{\uparrow\uparrow}(k_x)=\frac{v(k_x)}{\sqrt{w_{\uparrow\uparrow}(k_x)}}, \tag{3.6}$$

where $v(k_x)$ is the eigenvector of $\Lambda_{\uparrow\uparrow}$. When $n_{\mathrm{e}}=1$, the values of λ for $\uparrow\uparrow$ and $\downarrow\downarrow$ coincide, because of the particle-hole symmetry of the system. $\Delta_{\uparrow\uparrow}(k_x)$ and $\Delta_{\downarrow\downarrow}(k_x)$ do not coincide, but satisfy

$$\Delta_{\downarrow\downarrow}(k_x+\pi)=\Delta_{\uparrow\uparrow}(k_x), \tag{3.7}$$

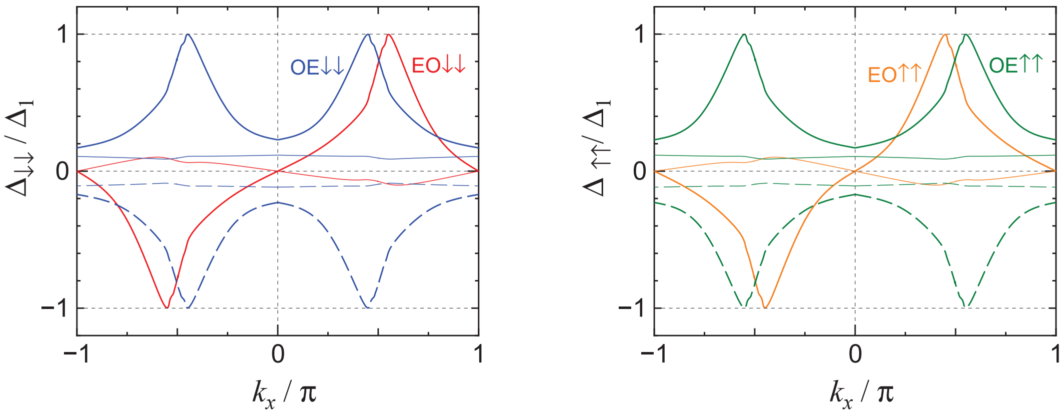

(a) (b)

Fig 3.2: Profiles of (a) $\Delta(k_x, \omega_n)$ and (b) $\Delta_{\uparrow\uparrow}(k_x, \omega_n)$ at the superconducting transition temperature. In panel (a), the red and blue curves show the results for EOT and OET states, respectively. In panel (b), the orange and green curves show the results for EO↑↑ and OE↑↑ states, respectively. We assume the isotropic Kondo coupling $J_{\rm K} = J_{\rm K}^{\parallel} = J_{\rm K}^{\perp}$. The value of J_K is assumed to be -0.31 for EO↓↓ and EO↑↑ states, whereas the value of J_K is assumed to be 0.28 for OE↓↓ and OE↑↑ states. These values are determined so that $\lambda = 1$ is satisfied at $T = 0.8T_{\rm FM}$. The thick and thin solid curves show the results for $\omega_n = \pi T$ and $3\pi T$, respectively, whereas the thick and thin dashed curves show the results for $\omega_n = -\pi T$ and $-3\pi T$, respectively. Either for the EO↓↓ or EO↑↑ state, the result for $-\omega_n$ coincides with that for ω_n. Δ_1 is the magnitude of the peak value for $\omega_n = \pm\pi T$. The panel (a) has been presented in Ref. [42].

independently of the pairing symmetry. The profiles of $\Delta_{\downarrow\downarrow}(k_x)$ and $\Delta_{\uparrow\uparrow}(k_x)$ reflect the structures of the order parameters near the transition temperature. We find that $\Delta_{\downarrow\downarrow}(k_x)$ and $\Delta_{\uparrow\uparrow}(k_x)$ have peaks near the Fermi momentum $k_{F\downarrow} \approx k_{F\uparrow} \approx 0.50\pi$.

3.3 Phase diagrams in J_{K}–T plane

3.3.1 Isotropic Kondo coupling

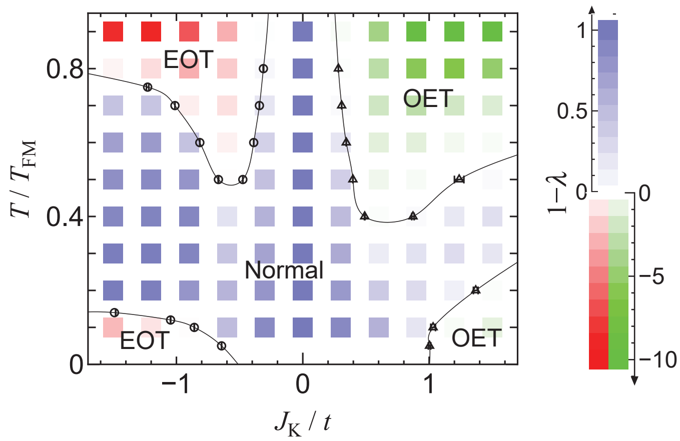

Fig 3.3: Phase diagram in J_{K}–T plane for isotropic Kondo coupling ($J_{\mathrm{K}}^{\perp} = J_{\mathrm{K}}^{\parallel}$). The color scale shows the minimum eigenvalue $1-\lambda$ at the center of the square. The blue squares show $1-\lambda > 0$ at the center of the square. The red squares show $1-\lambda < 0$ and the minimum eigenvalue occurs for the EOT state at the center of the square. The green squares show $1-\lambda < 0$ and the minimum eigenvalue occurs for the OET state at the center of the square. The open circles and triangles show the points where $\lambda = 1$. The solid curves are deduced from these results. This figure has been presented in Ref. [42].

In Fig. 3.3, the phase diagram in J_{K}–T plane is shown. Superconductivity occurs in high- and low-temperature regions. The normal region near $J_{\mathrm{K}} = 0$ extends to the large $|J_{\mathrm{K}}|$ region at intermediate temperatures. The OET and EOT states occur for $J_{\mathrm{K}} > 0$ and $J_{\mathrm{K}} < 0$, respectively. The normal region is wider for $J_{\mathrm{K}} < 0$ than for $J_{\mathrm{K}} > 0$. Antiparallel spin pairing does not occur, where the exchange field h is strong. Besides, $\Gamma^{(2)}_{\sigma,-\sigma}$ is repulsive for two electrons with antiparallel spins near the

Fermi surface in one dimension. However, $\Gamma^{(1)}_{\sigma,-\sigma}$ may induce antiparallel spin pairing where $|h|$ and $\Gamma^{(2)}_{\sigma,-\sigma}$ are small. From Eq. (2.27), $|h|$ is small at high temperatures or at small $|J_{\rm K}^{\parallel}|$. At high temperatures, $\Gamma^{(2)}_{\sigma,-\sigma}$ is large, since that involves the Bose distribution function. Therefore, antiparallel spin pairing may occur in the low-temperature and small $|J_{\rm K}^{\parallel}|$ region. $T_{\rm c} \lesssim T_{\rm FM} \approx 2.4 \times 10^{-3}$ and $|h| \approx 0.25|J_{\rm K}^{\parallel}|$, since $\langle S_i^z \rangle \approx 1/2$. Hence, $|J_{\rm K}^{\parallel}| \gtrsim 0.1$ gives sufficiently large $|h|$ that suppresses antiparallel spin pairing ($|h| \gtrsim 2.5 \times 10^{-2} \gg T_{\rm c}$). Therefore, antiparallel spin pairing can occur only in the limited region of $J_{\rm K}$ that satisfies $0.1 \gtrsim J_{\rm K} > 0$.

3.3.2 Ising-like Kondo coupling

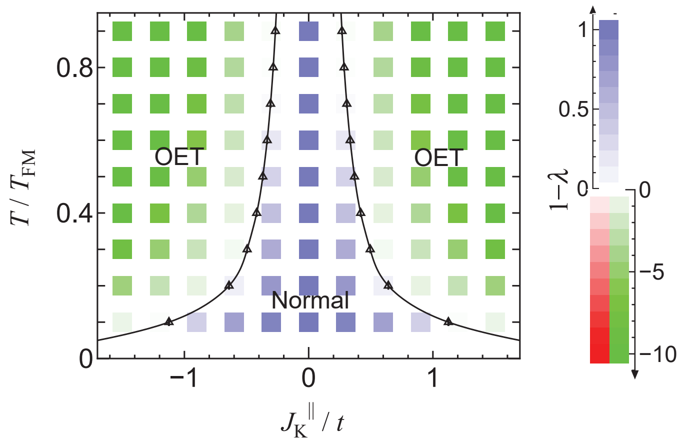

Fig 3.4: Similar to Fig. 3.3, but shows the phase diagram in $J_{\rm K}^{\parallel}$–T plane, for Ising-like Kondo coupling ($J_{\rm K}^{\perp} = 0$). This figure has been presented in Ref. [42].

Figure 3.4 shows the phase diagram when the Kondo coupling is Ising-like ($J_{\rm K}^{\perp} = 0$). In this case, $\Gamma^{(3)}_{\sigma\bar{\sigma}} \propto J_{\rm K}^{\parallel} {J_{\rm K}^{\perp}}^2 = 0$ vanishes and $\Gamma^{(2)}_{\sigma\sigma}$ remains. The OET state occurs in broad areas except near $J_{\rm K}^{\parallel} = 0$, whereas the EOT state disappears. At low temperatures, superconductivity does not occur, because the magnon density diminishes and $\Gamma^{(2)}_{\sigma\sigma}$ is weak. Antiparallel spin pairing does not occur even where $J_{\rm K}^{\parallel} \lesssim 0.1$, which was evaluated above because $\Gamma^{(1)}_{\sigma,-\sigma} \propto {J_{\rm K}^{\perp}}^2 = 0$ there, and $\Gamma^{(3)}_{\sigma\bar{\sigma}} \propto J_{\rm K}^{\parallel} {J_{\rm K}^{\perp}}^2 = 0$ in the present case.

3.4 Phase diagrams in $J_{\mathrm{K}}^{\parallel}$–$J_{\mathrm{K}}^{\perp}$ plane

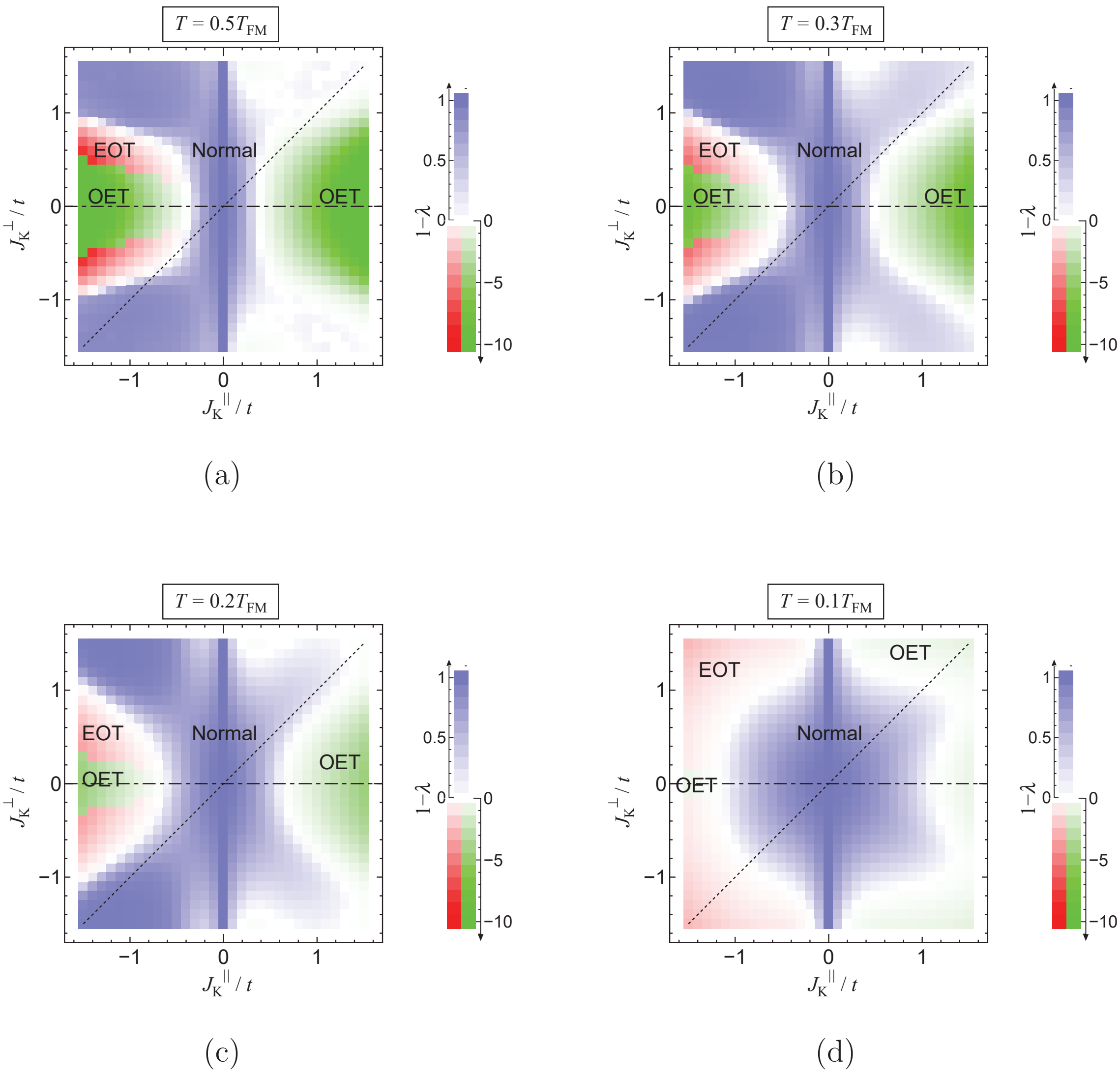

Fig 3.5: Similar to Fig. 3.3, but shows the phase diagram in $J_{\mathrm{K}}^{\parallel}$–$J_{\mathrm{K}}^{\perp}$ plane at $T = 0.5T_{\mathrm{FM}}, 0.3T_{\mathrm{FM}}, 0.2T_{\mathrm{FM}}$, and $0.1T_{\mathrm{FM}}$. On the dotted and dot-dashed lines, the Kondo coupling is isotropic and Ising-like, respectively. The panel (a) has been presented in Ref. [42].

Figure 3.5 shows the phase diagram in $J_{\mathrm{K}}^{\parallel}$–$J_{\mathrm{K}}^{\perp}$ plane at different temperatures below T_{FM}. In the phase diagrams at higher temperatures, the regions of superconductivity are large near the Ising line ($J_{\mathrm{K}}^{\perp} = 0$). The EOT state occurs only for $J_{\mathrm{K}}^{\parallel} < 0$. The OET state occurs independently of the sign of $J_{\mathrm{K}}^{\parallel}$. The phase boundaries between the EOT and OET states are inaccurate because they are determined by comparing the pairing susceptibilities calculated in the normal state. In the phase diagram at low temperature ($T = 0.1T_{\mathrm{FM}}$) shown in panel (d), the superconducting areas near the Ising line diminishes, but they extend to the large $|J_{\mathrm{K}}^{\perp}|$ region.

Let us discuss the possibility of antiparallel spin pairing again. For small $|J_{\mathrm{K}}^{\perp}|$, similarly to the Sec. 3.3.1, $|J_{\mathrm{K}}^{\parallel}| \gtrsim 0.1$ is sufficiently large to suppress antiparallel spin pairing. For large $|J_{\mathrm{K}}^{\perp}|$, however, the lower limit ($|J_{\mathrm{K}}^{\parallel}| \approx 0.1$) may not be large enough, because $\Gamma^{(1)}_{\sigma,-\sigma} \propto {J_{\mathrm{K}}^{\perp}}^2$. As $|J_{\mathrm{K}}^{\perp}|$ increases, the lower limit of $|J_{\mathrm{K}}^{\parallel}|$ increases.

3.5 $J^{\perp}$ dependence of the phase diagrams

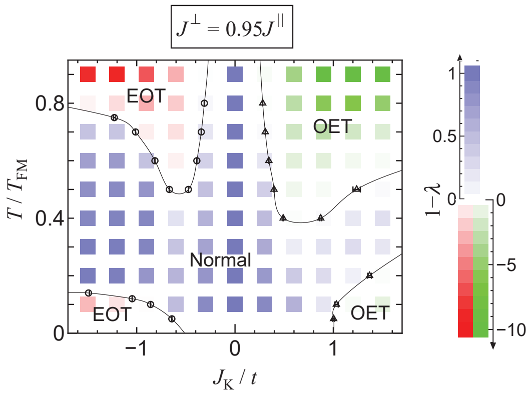

(a)

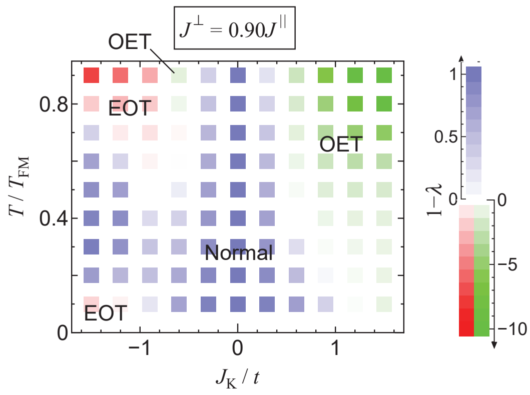

(b)

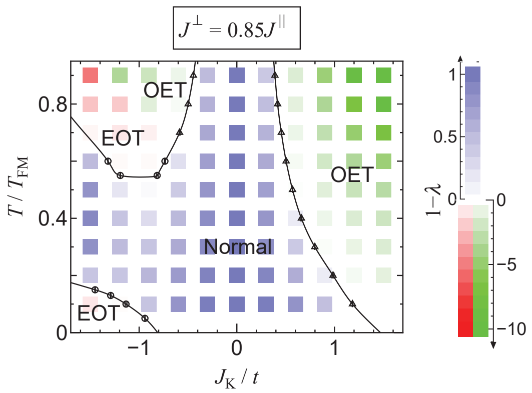

(c)

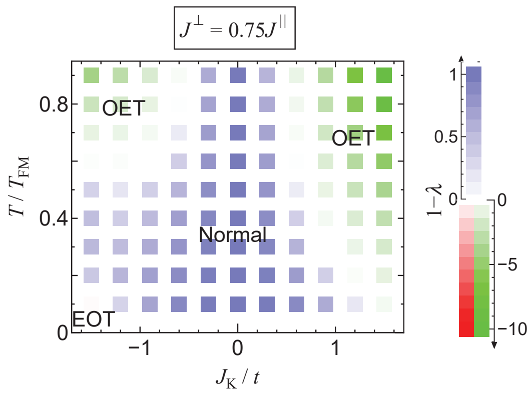

(d)

Fig 3.6: Similar to Fig. 3.3, but shows the results at several different $J^{\perp}$'s. Panels (a), (b), (c), and (d) are the results for $J^{\perp} = 0.95J^{\parallel}$, $0.9J^{\parallel}$, $0.85J^{\parallel}$, and $0.75J^{\parallel}$, respectively. Panel (a) is the same as Fig. 3.3.

In Fig. 3.6, we show the phase diagrams in J_{K}–T plane at $J^{\perp} = 0.95J^{\parallel}$, $0.9J^{\parallel}$, $0.85J^{\parallel}$, and $0.75J^{\parallel}$, for which the ferromagnetic transition temperatures are estimated as $T_{\mathrm{FM}} = 2.39 \times 10^{-3}$, 3.53×10^{-3}, 4.41×10^{-3}, and 5.73×10^{-3}, respectively. Isotropic Kondo coupling is assumed. In general, as $J^{\perp}/J^{\parallel}$ approaches to 1, the ferromagnetic fluctuation strengthens, and it is expected that superconductivity induced by the magnon-exchange interactions is enhanced. However, regarding the OET phase, the area in the phase diagram broaden as $J^{\perp}/J^{\parallel}$ decreases. Hence, for $J_{\mathrm{K}} > 0$, the areas of the high- and low-temperature OET phases merge in the phase diagrams for $J^{\perp} \lesssim 0.9J^{\parallel}$, and for $J_{\mathrm{K}} < 0$, the high-temperature EOT phase is gradually exclude by the OET phase as $J^{\perp}/J^{\parallel}$ decreases.

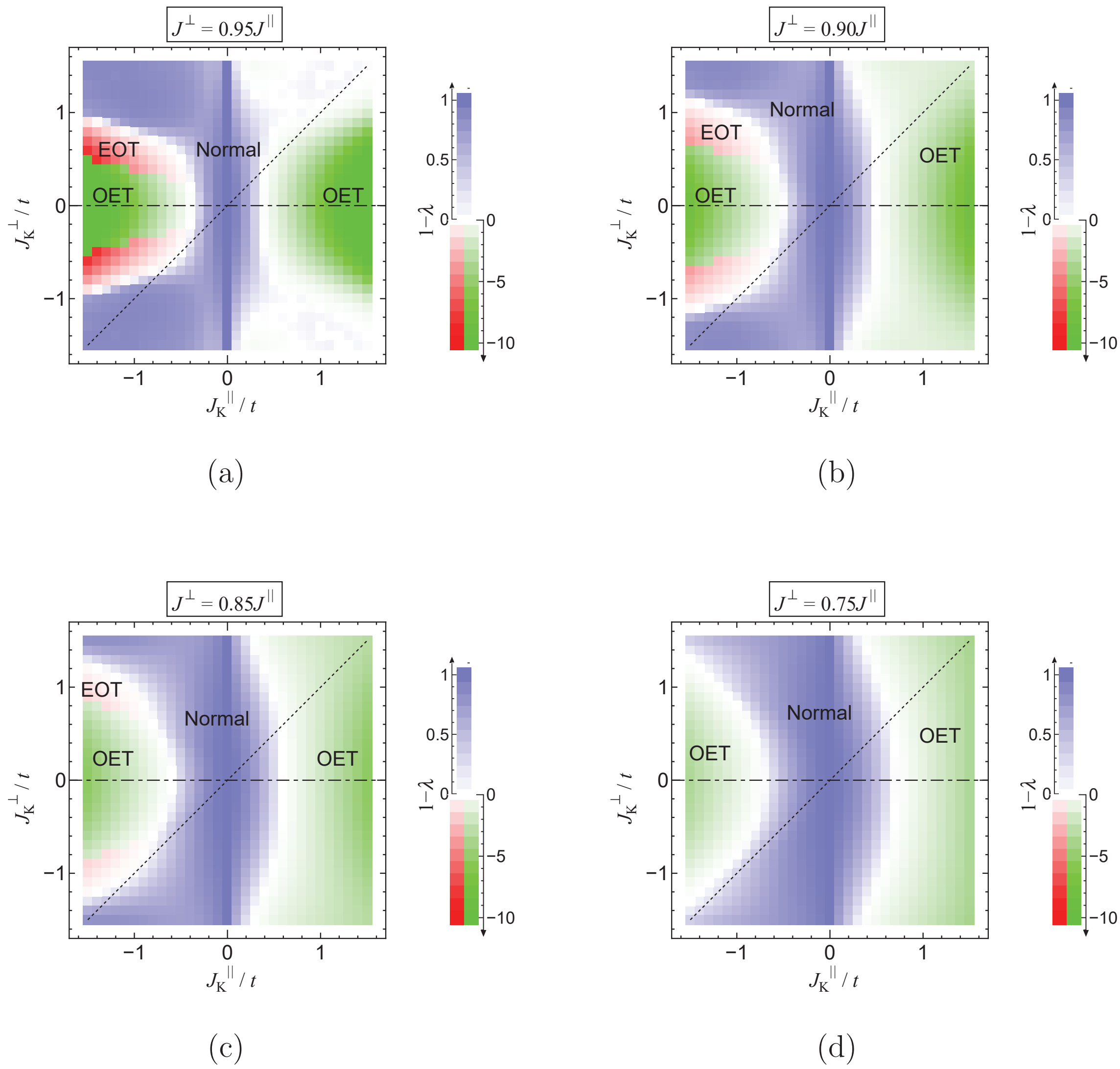

Fig 3.7: Similar to Fig. 3.5, but shows the results for several different $J^{\perp}$'s at $T = 0.5T_{\mathrm{FM}}$. Panels (a), (b), (c), and (d) are the results for $J^{\perp} = 0.95J^{\parallel}$, $0.9J^{\parallel}$, $0.85J^{\parallel}$, and $0.75J^{\parallel}$, respectively. Panel (a) is the same as Fig. 3.5 (a).

Figure 3.7 shows the phase diagrams in $J_{\mathrm{K}}^{\parallel}$–$J_{\mathrm{K}}^{\perp}$ plane at $T = 0.5T_{\mathrm{FM}}$ for several

$J^{\perp}$'s. As observed above, the area of the OET state enlarges as $J^{\perp}/J^{\parallel}$ decreases. The areas of the EOT state for $J_{\mathrm{K}} > 0$ shrink, as $J^{\perp}$ decreases.

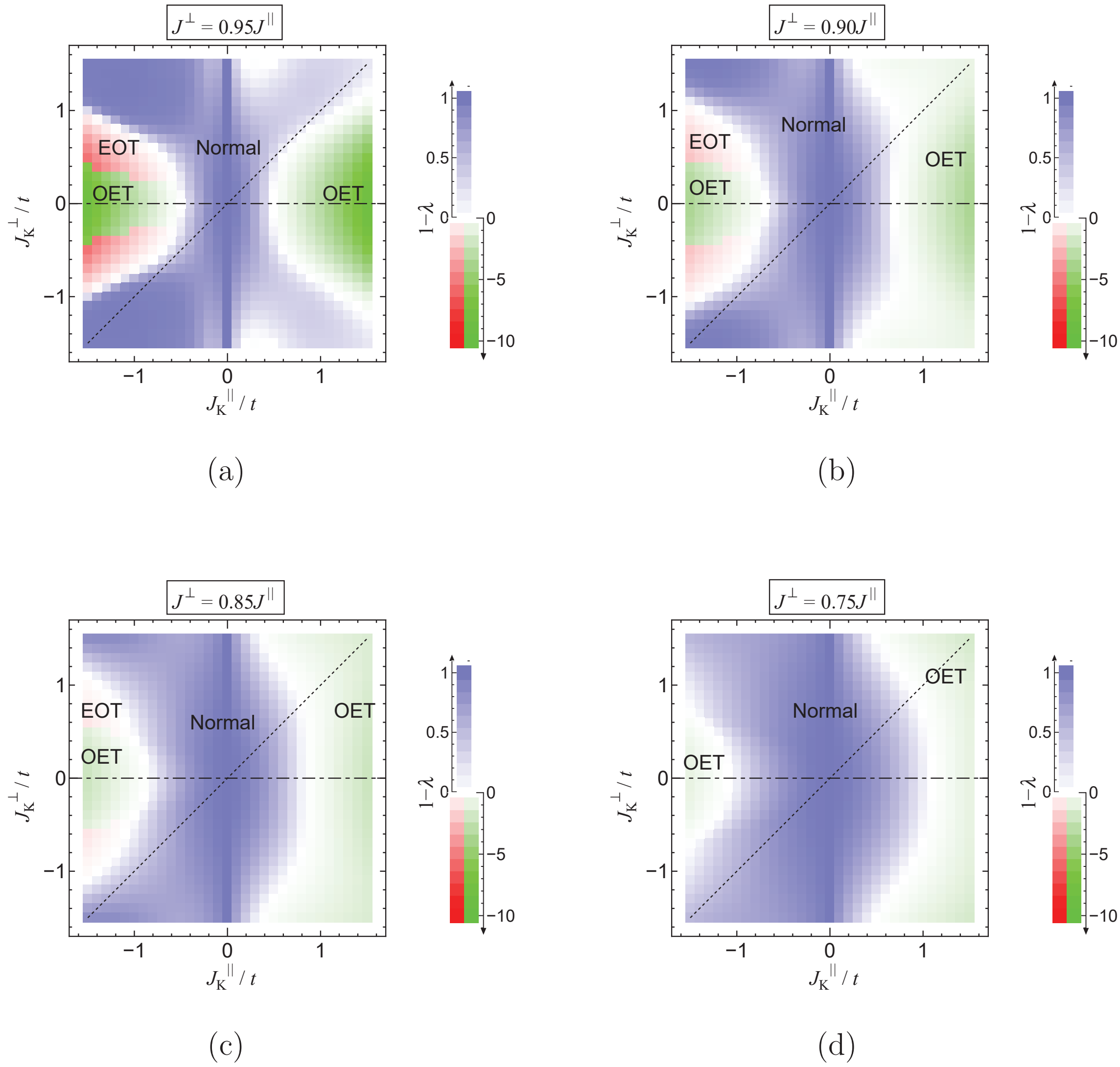

Fig 3.8: Similar to Fig. 3.5, but shows the results for several different $J^{\perp}$'s at $T = 0.3T_{\mathrm{FM}}$. Panels (a), (b), (c), and (d) are shown the results for $J^{\perp} = 0.95J^{\parallel}$, $0.9J^{\parallel}$, $0.85J^{\parallel}$, and $0.75J^{\parallel}$, respectively. Panel (a) is the same as Fig. 3.5 (b).

Figure 3.8 shows the phase diagrams at $T = 0.3T_{\mathrm{FM}}$. The results at $T = 0.5T_{\mathrm{FM}}$ are confirmed at this lower temperature.

Figure 3.9 shows the phase diagrams at $T = 0.1T_{\mathrm{FM}}$. As $J^{\perp}/J^{\parallel}$ approaches to 1, superconductivity is enhanced, as expected.

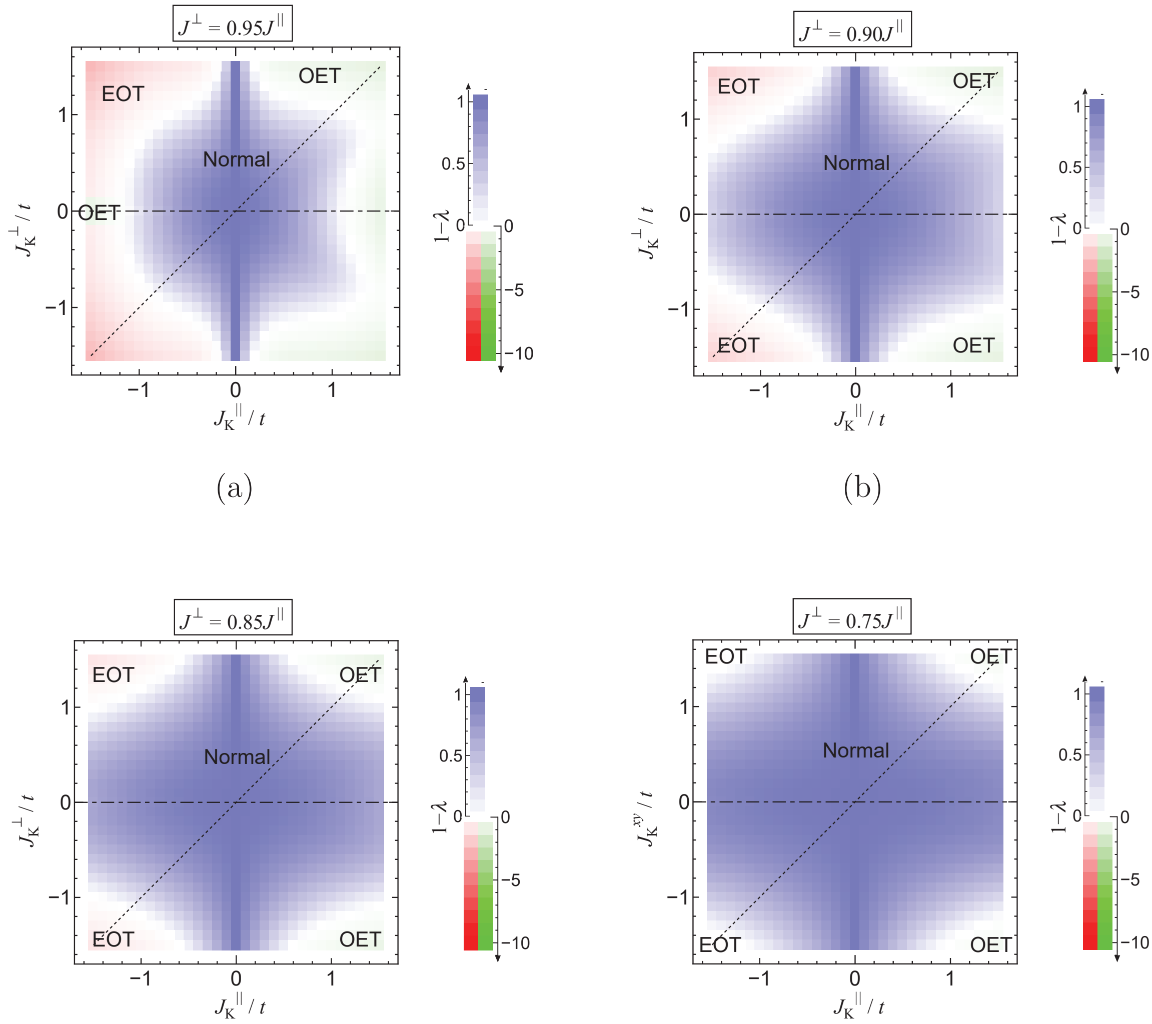

(a) (b) (c) (d)

Fig 3.9: Similar to Fig. 3.5, but shows the results for several different $J^{\perp}$'s at $T = 0.1T_{\mathrm{FM}}$. Panels (a), (b), (c), and (d) are shown the results for $J^{\perp} = 0.95J^{\parallel}$, $0.9J^{\parallel}$, $0.85J^{\parallel}$, and $0.75J^{\parallel}$, respectively. Panel (a) is the same as Fig. 3.5 (d).

3.6 $J^{\parallel}$ dependence of the phase diagrams

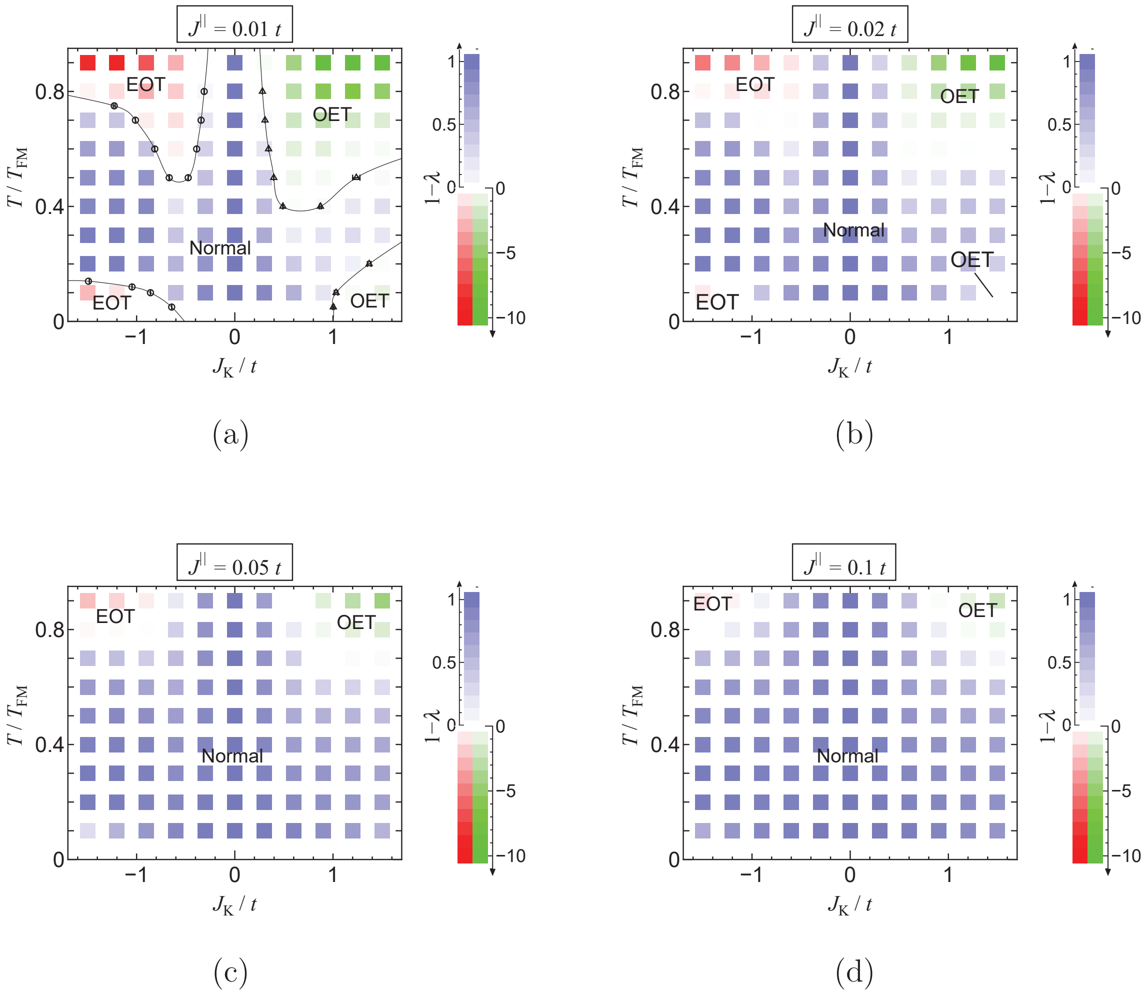

Fig 3.10: Similar to Fig. 3.3, but shows the results at several different $J^{\parallel}$'s. Panels (a), (b), (c), and (d) are the results for $J^{\parallel} = 0.01t$, $0.02t$, $0.05t$, and $0.1t$, respectively. Here, $J^{\perp} = 0.95J^{\parallel}$. Panel (a) is the same as Fig. 3.3.

In Fig. 3.10, we show the phase diagrams in $J_{\rm K}$–T plane at $J^{\perp} = 0.01t$, $0.02t$, $0.05t$, and $0.1t$, for which the ferromagnetic transition temperatures are estimated as $T_{\rm FM} = 2.39 \times 10^{-3}$, 4.77×10^{-3}, 1.19×10^{-2}, and 2.39×10^{-2}, respectively. Isotropic Kondo coupling is assumed. As $J^{\parallel}/t$ decreases, $T_{\rm FM}/t$ decreases, and it is expected that superconductivity is enhanced, because $\hat{W}_{\sigma\sigma}$ in Eq. (2.66) increases at low temperatures. These results are consistent with the expectations. The low-temperature superconducting areas disappear as $J^{\parallel}/t$ increases.

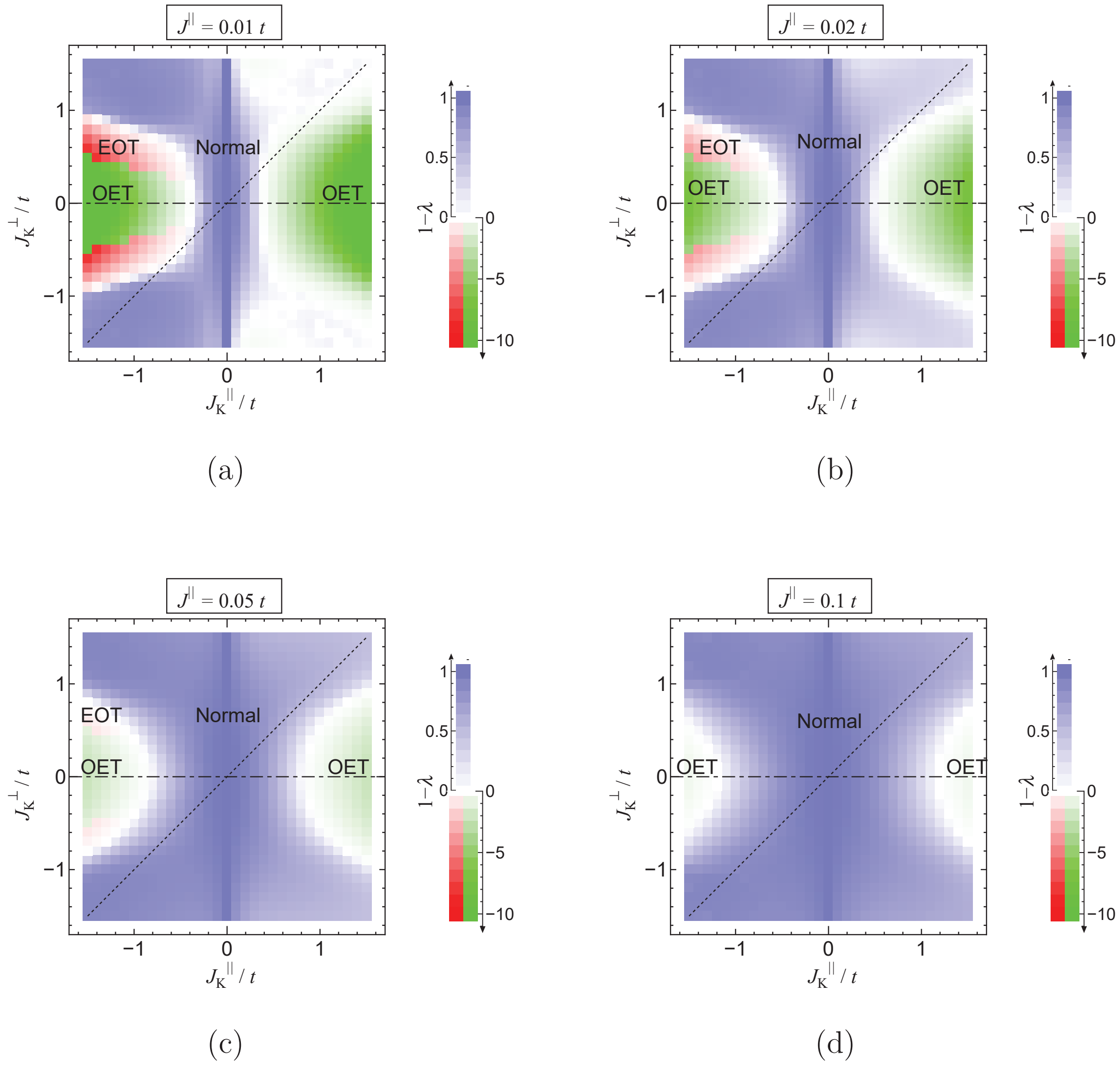

Fig 3.11: Similar to Fig. 3.5, but shows the results for several different $J^{\perp}$'s at $T = 0.5T_{\mathrm{FM}}$. Panels (a), (b), (c), and (d) are the results for $J^{\parallel} = 0.01t$, $0.02t$, $0.05t$, and $0.1t$, respectively. Here, $J^{\perp} = 0.95J^{\parallel}$. Panel (a) is the same as Fig. 3.5 (a).

Figure 3.11 shows the phase diagrams in $J_{\mathrm{K}}^{\parallel}$–$J_{\mathrm{K}}^{\perp}$ plane at $T = 0.5T_{\mathrm{FM}}$ for several $J^{\parallel}$'s. As $J^{\parallel}/t$ decreases, the superconducting areas enlarge. These results are consistent with the expectations.

Figure 3.12 shows the phase diagrams at $T = 0.1T_{\mathrm{FM}}$. As $J^{\parallel}/t$ increases, superconductivity is enhanced, as expected.

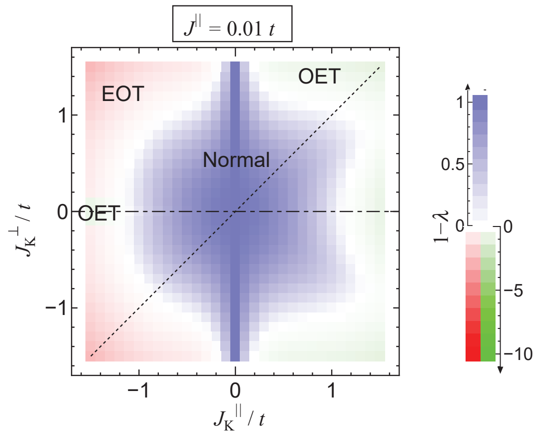

(a)

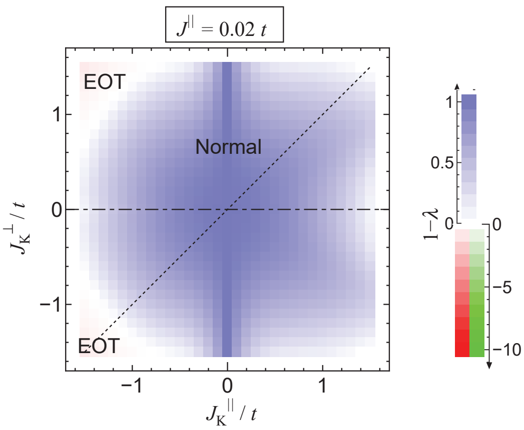

(b)

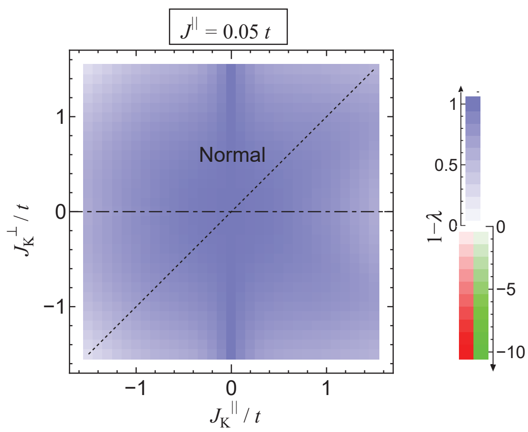

(c)

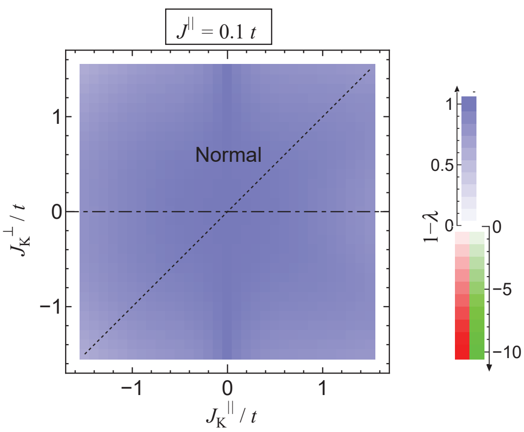

(d)

Fig 3.12: Similar to Fig. 3.5, but shows the results for several different $J^{\perp}$'s at $T = 0.1T_{\rm FM}$. Panels (a), (b), (c), and (d) are shown the results for $J^{\|} = 0.01t$, $0.02t$, $0.05t$, and $0.1t$, respectively. Here, $J^{\perp} = 0.95J^{\|}$. Panel (a) is the same as Fig. 3.5 (d).

3.7 n_e dependence of the phase diagrams

Figure 3.13 shows the phase diagrams for several n_e's at $J^\perp = 0.85J^\parallel$ and $T = 0.5T_\mathrm{FM}$. When $n_\mathrm{e} \neq 1$, the degeneracy of the values of λ for $\uparrow\uparrow$ and $\downarrow\downarrow$ spin pairings is removed. In the phase diagram, deeply inside the superconducting area, $\uparrow\uparrow$ and $\downarrow\downarrow$ spin pairing states coexist. In Figs. 3.13 and 3.14, only principal state is represented. As n_e decreases, the OE$\uparrow\uparrow$ and OE$\downarrow\downarrow$ phases are enhanced. In the phase diagram at $n_\mathrm{e} = 0.5$, the EO$\uparrow\uparrow$ phases disappear.

Figure 3.14 shows the phase diagrams for several n_e's at $J^\perp = 0.85J^\parallel$ and $T = 0.1T_\mathrm{FM}$. As n_e decreases, the superconducting areas enlarge. Odd-frequency superconductivity occurs when $J_\mathrm{K}^\parallel > 0$, whereas even-frequency superconductivity occurs when $J_\mathrm{K}^\parallel < 0$.

Figure 3.15 shows the phase diagrams for several n_e's at $J^\parallel = 0.02t$, $J^\perp = 0.95J^\parallel$, and $T = 0.5T_\mathrm{FM}$. As n_e decreases, the odd-frequency superconducting areas enlarge. When $J_\mathrm{K}^\parallel > 0$, the OET state occurs over large areas, because the OE$\downarrow\downarrow$ state occurs where $|J_\mathrm{K}^\perp|$ is large.

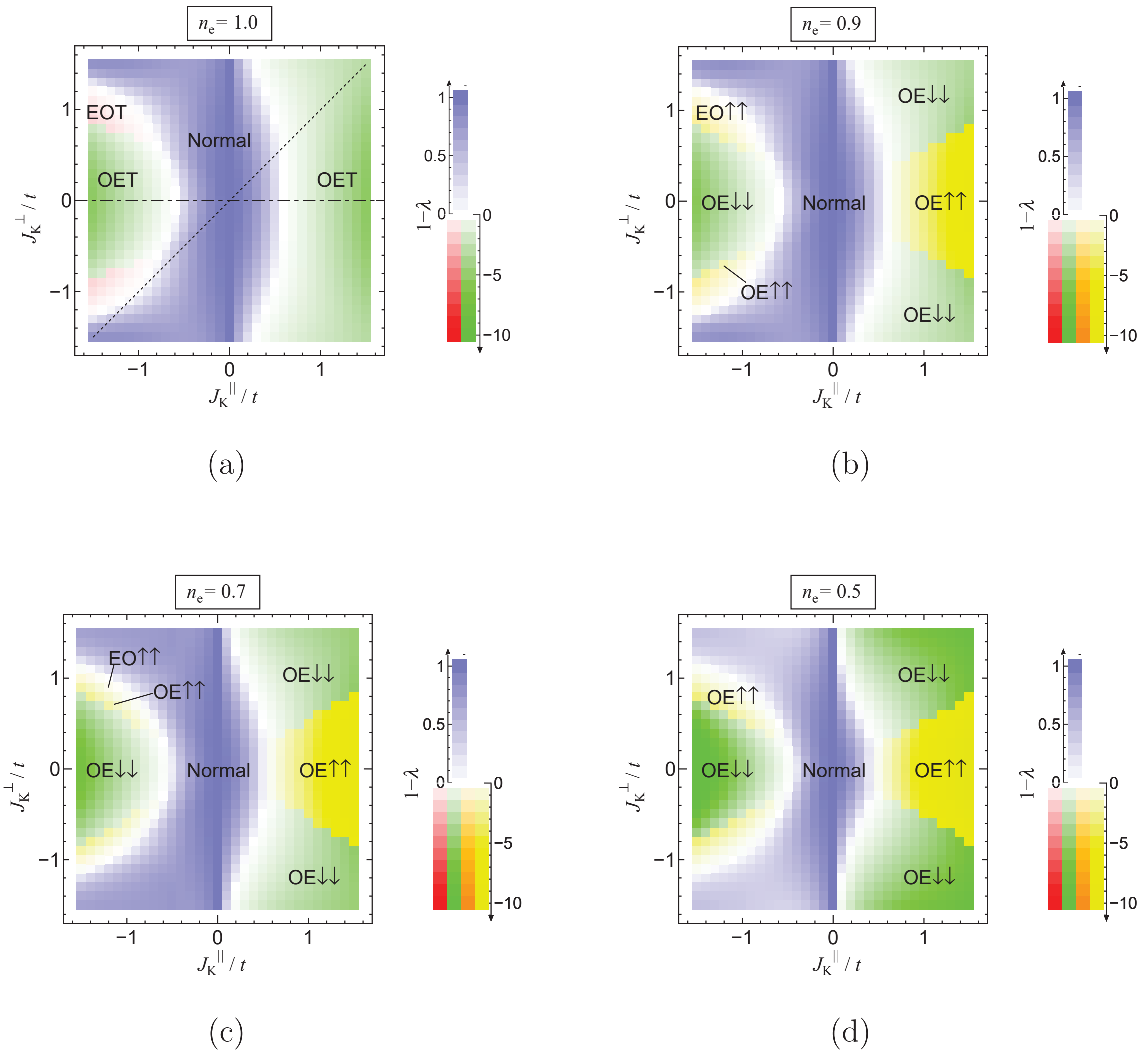

Fig 3.13: Similar to Fig. 3.5, but shows the results for several different n_e's at $T = 0.5T_{\mathrm{FM}}$. Panels (a), (b), (c), and (d) are shown the results for $n_e = 1.0$, 0.9, 0.7, and 0.5, respectively. Panel (a) is the same as Fig. 3.7 (c). The red, orange, green, and yellow squares show the minimum eigenvalue occur for the EO↓↓, EO↑↑, OE↓↓, and OE↑↑ states at the center of the square, respectively.

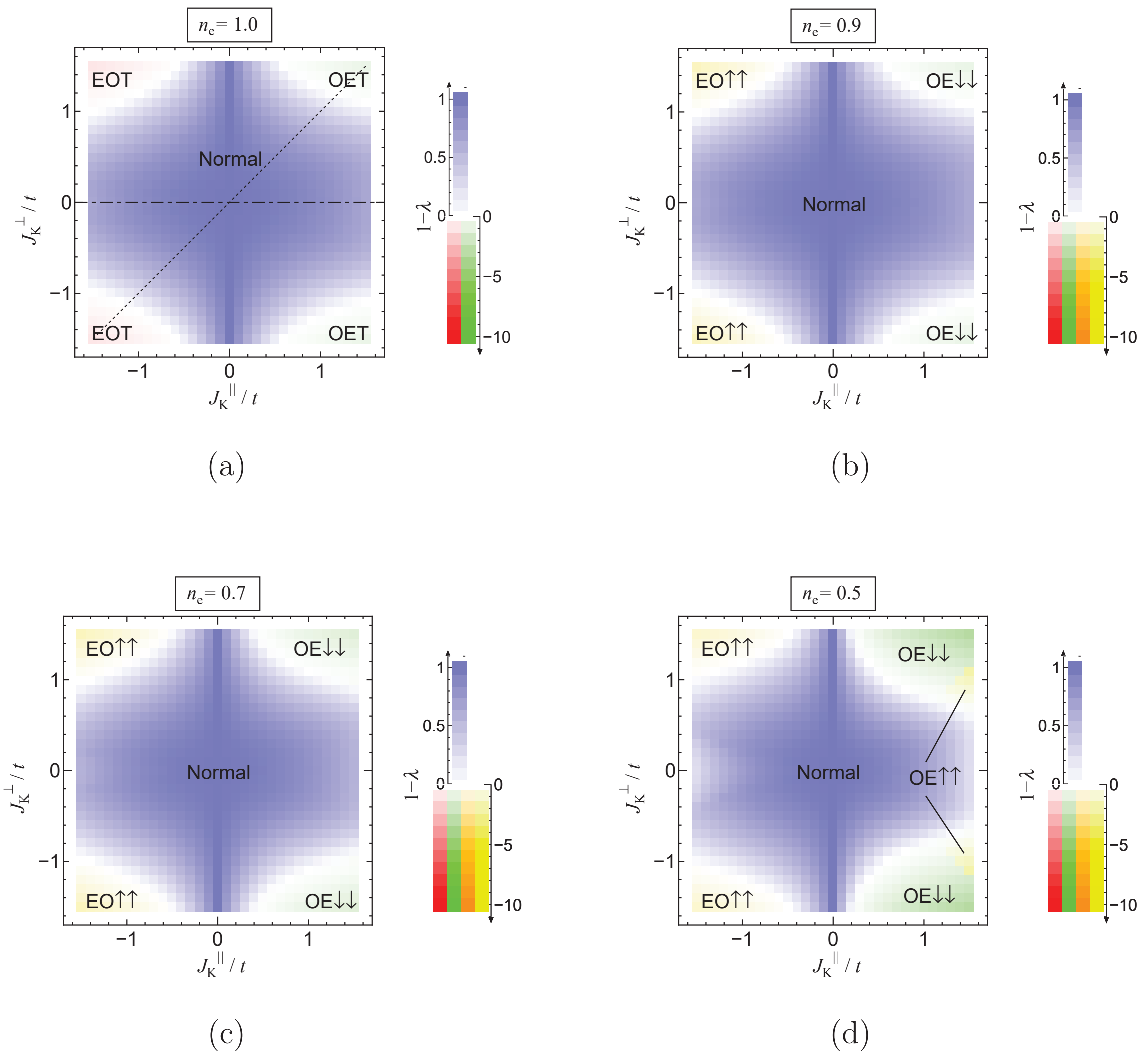

Fig 3.14: Similar to Fig. 3.13, but shows the results at $T = 0.1T_{\mathrm{FM}}$. Panels (a), (b), (c), and (d) are shown the results for $n_{\mathrm{e}} = 1.0$, 0.9, 0.7, and 0.5, respectively. Panel (a) is the same as Fig. 3.9 (c).

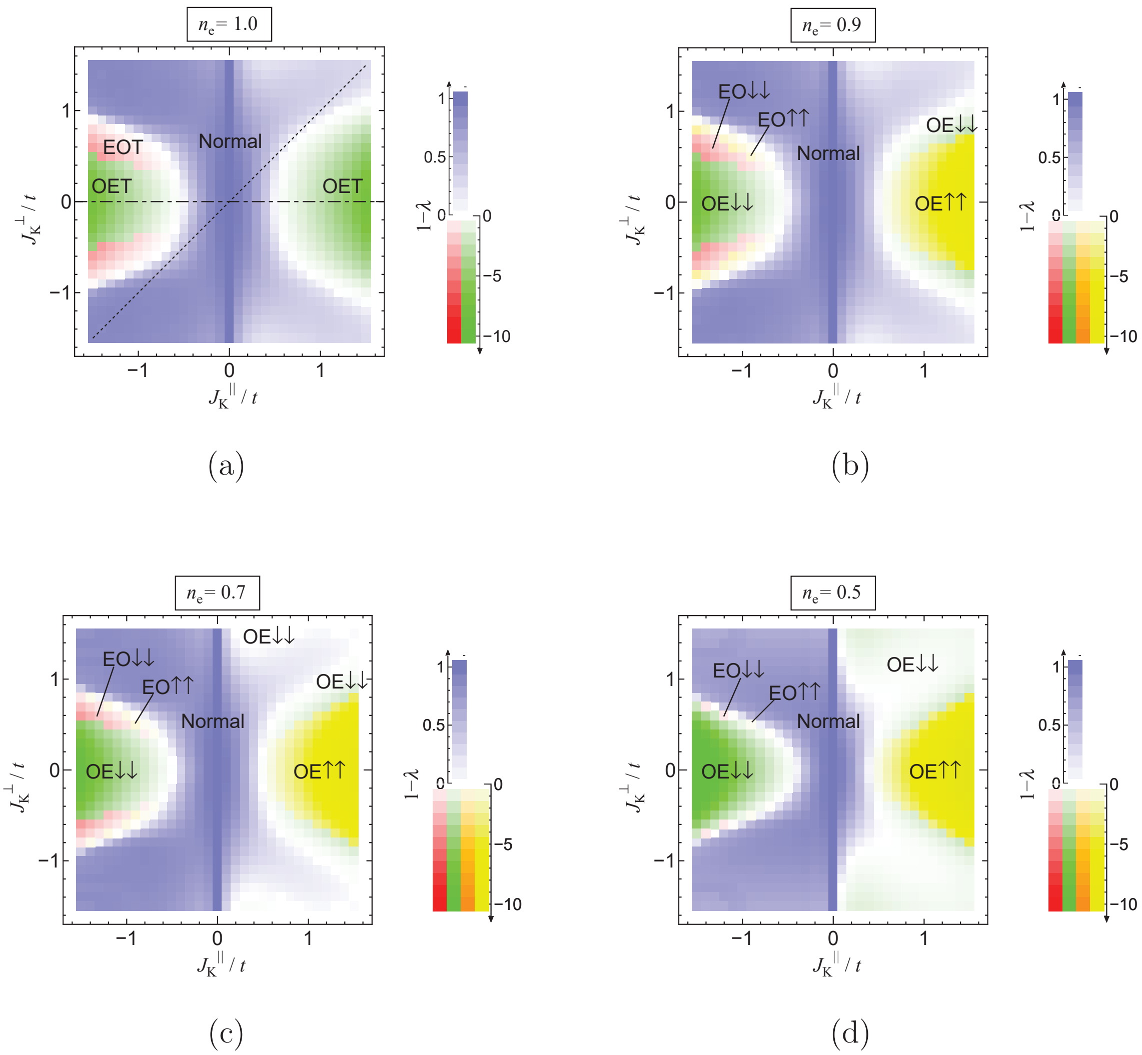

Fig 3.15: Similar to Fig. 3.13, but shows the results for $J^{\parallel} = 0.02t$, $J^{\perp} = 0.95J^{\parallel}$, and $T = 0.5T_{\rm FM}$. Panels (a), (b), (c), and (d) are shown the results for $n_{\rm e} = 1.0$, 0.9, 0.7, and 0.5, respectively. Panel (a) is the same as Fig. 3.11 (b).

Chapter 4

Summary and Discussion

4.1 Properties of the two-magnon-exchange interactions

An interesting feature of the two-magnon-exchange interactions depicted in Fig. 2.1 (b) is the strong spin dependence. It is verified from Eq. (2.59) that $\Gamma^{(2)}_{\sigma\sigma}$ is attractive, whereas $\Gamma^{(2)}_{\sigma,-\sigma}$ is repulsive, at any (k,k'). The part of $\Gamma^{(2)}_{\sigma\bar{\sigma}}$ after the prefactor $\sigma\bar{\sigma}$ is positive, because $n(\omega_{\boldsymbol{k}_1-\boldsymbol{k}'})-n(\omega_{\boldsymbol{k}_1-\boldsymbol{k}})<0$ when $\omega_{\boldsymbol{k}_1-\boldsymbol{k}'}-\omega_{\boldsymbol{k}_1-\boldsymbol{k}}>0$. Since $\Gamma_{\sigma\sigma}(k,k')$ is positive, it contributes to $\chi^{\alpha(\pm)}_{\sigma\sigma}$ as an attractive interaction. In contrast, $\Gamma^{(2)}_{\sigma,-\sigma}$ is repulsive. Hence, particularly in one-dimension, antiparallel spin pairing is strongly suppressed, because $|\Gamma^{(2)}_{\sigma-\sigma}|$ is large at $k=k'$.

	Coupling constant	$T=0$
$\Gamma^{(2)}_{\sigma\sigma}$	${J_{\mathrm{K}}^{\parallel}}^2$	0
$\Gamma^{(3)}_{\sigma\sigma}$	$J_{\mathrm{K}}^{\parallel}{J_{\mathrm{K}}^{\perp}}^2$	$\neq 0$

Table 4.1: Coupling constants in $\Gamma^{(2)}_{\sigma\sigma}$ and $\Gamma^{(3)}_{\sigma\sigma}$, and their behaviors at $T=0$.

Anisotropy in the Kondo coupling also gives rise to essential difference in the pairing symmetry. From Eqs. (2.59) and (2.61), we summarize the relation between the coupling constants and the behaviors at $T=0$ in Table 4.1. Because $\Gamma^{(3)}_{\sigma\sigma}=0$ when $J_{\rm K}^{\perp}=0$, and $J_{\rm K}^{\perp}$ appears only in the coupling constant of $\Gamma^{(3)}_{\sigma\sigma}$, we can take the phase diagram of Fig. 3.4 for Ising-like Kondo coupling ($J_{\rm K}^{\perp}=0$) as that for isotropic Kondo coupling where $\Gamma^{(3)}_{\sigma\sigma}$ is ignored. Therefore, we find that the OET phases in Fig. 3.4 are induced by $\Gamma^{(2)}_{\sigma\sigma}$. In the present theory, $J_{\rm K}^{\parallel}$ appears in both the coupling constant and the exchange field h. However, because $\Gamma^{(2)}_{\sigma\sigma}$ does not depend on h, $\Gamma^{(2)}_{\sigma\sigma}\propto {J_{\rm K}^{\parallel}}^2$ does not depend on the sign of $J_{\rm K}^{\parallel}$. The normal phase is stable at low temperatures, because the OET state is induced by $\Gamma^{(2)}_{\sigma\sigma}$, and $\Gamma^{(2)}_{\sigma\sigma}\to 0$ in the limit $T\to 0$. All terms of $\Gamma^{(2)}_{\sigma\sigma}$ are proportional to the Bose distribution function, which vanishes at $T=0$.

Near the Ising line ($\Gamma^{(3)}_{\sigma,\bar{\sigma}}\propto J_{\rm K}^{\parallel}{J_{\rm K}^{\perp}}^2=0$), in the phase diagrams in the $J_{\rm K}^{\parallel}$–$J_{\rm K}^{\perp}$ plane, the strongest interaction that contributes to the superconductivity is $\Gamma^{(2)}_{\sigma\sigma}$. For example, in Fig. 3.5, the OET phases near the Ising line are induced by $\Gamma^{(2)}_{\sigma\sigma}$.

$\Gamma^{(2)}_{\sigma\sigma}$ decreases when $J^{\perp}$ decreases. From the expression of $\omega_{\boldsymbol{q}}$ Eq. (3.2), when $J^{\perp}$ decreases, the magnon bandwidth $J^{\perp}$ decreases, and the energy gap $J^{\parallel}-J^{\perp}$ increases. Hence, the Bose distribution function decreases, and thus $\Gamma^{(2)}_{\sigma\sigma}$ decreases. In the phase diagrams at $T=0.5T_{\rm FM}$ shown in Fig. 3.7, on the Ising line ($\Gamma^{(3)}_{\sigma,\bar{\sigma}}\propto J_{\rm K}^{\parallel}{J_{\rm K}^{\perp}}^2=0$), as $J^{\perp}$ decreases, the region of the normal phase extends to the large $|J_{\rm K}^{\parallel}|$ region. At low temperatures such as $T=0.1T_{\rm FM}$, as $J^{\perp}$ decreases, the OET phases near the Ising line disappear, because $\Gamma^{(2)}_{\sigma\sigma}$ is too small.

When $n_{\rm e}\neq 1$, $\Gamma^{(2)}_{\sigma\sigma}$ induces the OE↑↑ and OE↓↓ states when $J_{\rm K}^{\parallel}>0$ and $J_{\rm K}^{\parallel}<0$, respectively. This dependence on the sign of $J_{\rm K}^{\parallel}$ originates from $w_{\sigma\sigma}$, which depends on $J_{\rm K}^{\parallel}$ through $\xi_{\boldsymbol{k}\sigma}$, but not from $\Gamma^{(2)}_{\sigma\sigma}$ itself, because $\Gamma^{(2)}_{\sigma\sigma}$ does not depend on the sign of $J_{\rm K}^{\parallel}$. For example, this behavior explicitly appears on the Ising line in the phase diagrams at $T=0.5T_{\rm FM}$ in Fig. 3.13, because $\Gamma^{(3)}_{\sigma,\bar{\sigma}}\propto J_{\rm K}^{\parallel}{J_{\rm K}^{\perp}}^2=0$ on this line.

$\Gamma^{(2)}_{\sigma\sigma}$ and $\Gamma^{(3)}_{\sigma\sigma}$ cooperatively induce the OE↑↑ state at small $n_{\rm e}$ such as $n_{\rm e}=0.5$. $\Gamma^{(2)}_{\sigma\sigma}$ does not depend on $n_{\rm e}$, while $\Gamma^{(3)}_{\sigma\sigma}$ and $w_{\sigma\sigma}$ depend on it. Looking at the phase diagrams at $T=0.1T_{\rm FM}$ shown in Fig. 3.14, the superconducting phases near the

Ising line disappear. However, in the phase diagram at $n_{\mathrm{e}} = 0.5$, the OE$\uparrow\uparrow$ state occurs where $J_{\mathrm{K}}^{\parallel}$ is large positive near the Ising line.

4.2 Properties of the interactions induced by triangle processes

Because $\Gamma_{\sigma\sigma}^{(3)}$ has a prefactor $J_{\mathrm{K}}^{\parallel} {J_{\mathrm{K}}^{\perp}}^2$ as shown in table 4.1, $\Gamma_{\sigma\sigma}^{(3)}$ changes the sign when the sign of $J_{\mathrm{K}}^{\parallel}$ changes, in contrast to $\Gamma_{\sigma\sigma}^{(2)}$. As a result, the effective interaction $\Gamma_{\sigma\sigma}^{(3)}$ can be attractive for the EOT state when $J_{\mathrm{K}}^{\parallel} < 0$, but repulsive when $J_{\mathrm{K}}^{\parallel} > 0$, as illustrated in Fig. 3.3 for the isotropic Kondo coupling. However, when $J_{\mathrm{K}}^{\perp} = 0$, $\Gamma_{\sigma\sigma}^{(3)}$ does not work, because the prefactor $J_{\mathrm{K}}^{\parallel} {J_{\mathrm{K}}^{\perp}}^2$ vanishes. Hence, the EOT state does not appear in Fig. 3.4 for Ising-like Kondo coupling ($J_{\mathrm{K}}^{\perp} = 0$). This behavior is clearly shown in the phase diagrams in $J_{\mathrm{K}}^{\parallel}$–$J_{\mathrm{K}}^{\perp}$ plane (Fig. 3.5). The EOT state occurs only in the region with $J_{\mathrm{K}}^{\parallel} < 0$. In panels (a), (b), and (c), the EOT state occurs in the region between the region of the OET state and the normal state.

In the intermediate-temperature region, $\Gamma_{\sigma\sigma}^{(3)}$ is repulsive. Because $\Gamma_{\sigma\sigma}^{(3)}$ has the terms proportional to the Bose distribution function and the terms proportional to the Fermi distribution function, $\Gamma_{\sigma\sigma}^{(3)}$ has complicated T dependence. In Fig. 3.3, at intermediate temperatures, the region of the normal phase extends to large $|J_{\mathrm{K}}|$. In Fig. 3.5, superconductivity is suppressed by $\Gamma_{\sigma\sigma}^{(3)}$ in the region where $|J_{\mathrm{K}}^{\parallel}|$ and $|J_{\mathrm{K}}^{\perp}|$ are large, at intermediate temperatures such as $T = 0.5T_{\mathrm{FM}}$, $0.3T_{\mathrm{FM}}$, and $0.2T_{\mathrm{FM}}$. As an exceptional case, $\Gamma_{\sigma\sigma}^{(3)}$ induces the OET state where $J_{\mathrm{K}}^{\parallel}$ is small positive and $|J_{\mathrm{K}}^{\perp}|$ is large.

In the low-temperature region, the strongest interaction that contributes to the superconductivity is $\Gamma_{\sigma\sigma}^{(3)}$. In Fig. 3.3, in the limit $T \to 0$, the superconducting phases induced by $\Gamma_{\sigma\sigma}^{(3)}$ remain. In Fig. 3.5 (d), $\Gamma_{\sigma\sigma}^{(3)}$ induces superconductivity over large areas in the parameter space. The superconducting state occurs where $|J_{\mathrm{K}}^{\parallel}|$ is small and $|J_{\mathrm{K}}^{\perp}|$ is large. This behavior is different from that of the superconducting state induced by $\Gamma^{(2)}_{\sigma\sigma}$.

Now, we discuss $J^{\perp}/J^{\parallel}$ dependence of $\Gamma^{(3)}_{\sigma\sigma}$. The magnetic fluctuations become stronger as $J^{\perp}/J^{\parallel}$ approaches 1. Therefore, the pairing interactions mediated by the magnetic fluctuations are strong near $J^{\perp}/J^{\parallel} = 1$.

$\Gamma^{(3)}_{\sigma\sigma}$ is enhanced more strongly than $\Gamma^{(2)}_{\sigma\sigma}$, when $J^{\perp}/J^{\parallel}$ approaches 1. The phase diagrams in $J_{\rm K}$–T plane for $J^{\perp} \leq 0.95J^{\parallel}$ are shown in Fig. 3.6. Where $J^{\parallel}_{\rm K} < 0$, in the high-temperature region, the area of the EOT phase induced by $\Gamma^{(3)}_{\sigma\sigma}$ broadens as $J^{\perp}$ increases. Similarly, in the phase diagram in $J^{\parallel}_{\rm K}$–$J^{\perp}_{\rm K}$ plane, which is shown by Fig. 3.7, the EOT areas broaden as $J^{\perp}$ increases. In the phase diagram at $T = 0.1T_{\rm FM}$ (Fig. 3.9), the superconducting states occupy broad regions for $J^{\perp}/J^{\parallel} = 0.95$, but those regions shrink when $J^{\perp}/J^{\parallel}$ decreases as expected from above argument.

In the intermediate-temperature region, $\Gamma^{(3)}_{\sigma\sigma}$ and $\Gamma^{(2)}_{\sigma\sigma}$ are competitive at large value of $J^{\perp}$, such as $J^{\perp} = 0.95J^{\parallel}$. However, when $J^{\parallel}_{\rm K} > 0$, they are cooperative at small value of $J^{\perp}$, such as $J^{\perp} = 0.9J^{\parallel}$. In the phase diagrams in Fig. 3.6 except that at $J^{\perp} = 0.95J^{\parallel}$, the OET state occurs in the whole temperature region, when $J^{\parallel}_{\rm K} > 0$. In the phase diagrams in Fig. 3.7 except that at $J^{\perp} = 0.95J^{\parallel}$, the OET state occurs over large areas, when $J^{\parallel}_{\rm K} > 0$. The normal phase near the isotropic line ($J^{\perp}_{\rm K} = J^{\parallel}_{\rm K}$) disappears.

When $n_{\rm e} \neq 1$, $\Gamma^{(3)}_{\sigma\sigma}$ induces the OE$\downarrow\downarrow$ and the EO$\uparrow\uparrow$ states where $J^{\parallel}_{\rm K} > 0$ and $J^{\parallel}_{\rm K} < 0$, respectively. The phase diagrams at $n_{\rm e} \neq 1$ are similar to the phase diagram at $n_{\rm e} = 1$, but the values of the pairing susceptibility for up-up and down-down spin pairing are not equal, because the particle-hole symmetry is broken. For example, this behavior appears in the phase diagrams for $T = 0.1T_{\rm FM}$ in Fig. 3.14.

At intermediate temperatures such as $T = 0.5T_{\rm FM}$, $\Gamma^{(3)}_{\sigma\sigma}$ and $\Gamma^{(2)}_{\sigma\sigma}$ are competitive where $J^{\parallel}_{\rm K} < 0$. Therefore, it is hard to say which state is more stable a priori. By a numerical calculation, we find that the OE$\uparrow\uparrow$ state occurs in the region between the region of the EO$\uparrow\uparrow$ and the OE$\downarrow\downarrow$ states in Fig. 3.13 where $J^{\parallel}_{\rm K} < 0$.

We ignored antiparallel spin pairing, which can occur where $|J^{\perp}_{\rm K}|$ is large and $|J^{\parallel}_{\rm K}|$

is small. We also ignored the self energy, which would decrease the superconducting transition temperature. Furthermore, in two and three dimensions, the phase diagrams would be different from those for quasi-one dimension, which were obtained in this thesis. These problems are left for future research.

4.3 Conclusion

We examined superconductivity mediated by ferromagnetic magnons on the basis of the generalized Kondo lattice model. Adopting the perturbation theory and diagram technique developed by Feynman, we derived the effective pairing interactions. We took into account not only the second order term $\Gamma^{(2)}_{\sigma\sigma}$, but also the third order term $\Gamma^{(3)}_{\sigma\sigma}$. We calculated the pairing susceptibility fully taking into account the spatial and temporal dependences in quasi-one-dimension. As a result, we revealed the emergence of both even- and odd-frequency superconductivities. At high temperatures but below T_{FM}, the two-magnon-exchange interactions $\Gamma^{(2)}_{\sigma\sigma}$ favor odd-frequency superconductivity near the region where Kondo coupling is Ising-like. At low temperatures, the interactions induced by triangle processes $\Gamma^{(3)}_{\sigma\sigma}$ induce odd- and even-frequency superconductivities near the region where Kondo coupling is isotropic. $\Gamma^{(3)}_{\sigma\sigma}$ induces odd- and even-frequency superconductivities, when Kondo coupling is antiferromagnetic ($J_{\mathrm{K}} > 0$) and ferromagnetic ($J_{\mathrm{K}} < 0$), respectively. The present results suggest that odd-frequency superconductivity occurs in a ferromagnetic superconductor as a bulk homogeneous state.

Reference

[1] W. A. Fertig, D. C. Johnston, L. E. DeLong, R. W. McCallum, M. B. Maple, and B. T. Matthias, Phys. Rev. Lett. **38**, 987 (1977).

[2] D. E. Moncton, D. B. McWhan, P. H. Schmidt, G. Shirane, W. Thomlinson, M. B. Maple, H. B. MacKay, L. D. Woolf, Z. Fisk, and D. C. Johnston, Phys. Rev. Lett. **45**, 2060 (1980).

[3] M. Ishikawa and O. Fischer, Solid State Commun. **23**, 37 (1977).

[4] J. W. Lynn, G. Shirane, W. Thomlinson, R. N. Shelton, and D. E. Moncton, Phys. Rev. B **24**, 3817 (1981).

[5] S. S. Saxena, P. Agarwal, K. Ahilan, F. M. Grosche, R. Haselwimmer, M. Steiner, E. Pugh, I. Walker, S. Julian, P. Monthoux, G. Lonzarich, A. Huxley. I. Sheikin, D. Braithwaite, and J. Flouquet, Nature (London) **406**, 587 (2000).

[6] D. Aoki, A. Huxley, E. Ressouche, D. Braithwaite, J. Flouquet, J.-P. Brison, E. Lhotel, and C. Paulsen, Nature (London) **413**, 613 (2001).

[7] N. T. Huy, A. Gasparini, D. E. de Nijs, Y. Huang, J. C. P. Klaasse, T. Gortenmulder, A. de Visser, A. Hamann, T. Görlach, and H. v. Löhneysen, Phys. Rev. Lett. **99**, 067006 (2007).

[8] D. Aoki and J. Flouquet, J. Phys. Soc. Jpn. **81**, 011003 (2012).

[9] H. Shimahara, J. Phys. Soc. Jpn. **63**, 1861 (1994).

[10] N. I. Karchev, K. B. Blagoev, K.S. Bedell, and P. B. Littlewood, Phys. Rev. Lett. **86**, 846 (2001).

[11] N. Karchev, Phys. Rev. B **67**, 054416 (2003).

[12] K. Hattori and H. Tsunetsugu, Phys. Rev. B **87**, 064501 (2013).

[13] V. L. Berezinskii, Pis'ma Zh. Eksp. Teor. Fiz. **20**, 628 (1974) [translation: Sov. Phys. JETP, **20**, 287 (1974)].

[14] A. Balatsky and E. Abrahams, Phys. Rev. B **45**, 13125 (1992).

[15] E. Abrahams, A. Balatsky, D. J. Scalapino, and J. R. Schrieffer, Phys. Rev. B **52**, 1271 (1995).

[16] D. Solenov, I. Martin, and D. Mozyrsky, Phys. Rev. B **79**, 132502 (2009).

[17] H. Kusunose, Y. Fuseya, and K. Miyake, J. Phys. Soc. Jpn. **80**, 054702 (2011).

[18] P. Coleman, E. Miranda, and A. Tsvelik, Phys. Rev. Lett. **70**, 2960 (1993); P. Coleman, E. Miranda, and A. Tsvelik, Phys. Rev. B **49**, 8955 (1994).

[19] M. Vojta and E. Dagotto, Phys. Rev. B **59**, 713 (1999).

[20] Y. Fuseya, H. Kohno and K. Miyake, J. Phys. Soc. Jpn. **72**, 2914 (2003).

[21] K. Shigeta, S. Onari, K. Yada, and Y. Tanaka, Phys. Rev. B **79**, 174507 (2009).

[22] H. Kusunose, Y. Fuseya, and K. Miyake, J. Phys. Soc. Jpn. **80**, 044711 (2011).

[23] F. S. Berget, A. F. Volkov, and K. B. Efetov, Phys. Rev. Lett. **86**, 4096 (2001); F. S. Berget, A. F. Volkov, and K. B. Efetov, Rev. Mod. Phys. **77**, 1321 (2005).

[24] Y. Asano, Y. Sawa, Y. Tanaka, and A. A. Golubov, Phys. Rev. B **76**, 224525 (2007).

[25] T. Yokoyama, Y. Tanaka, and A. A. Golubov, Phys. Rev. B **75**, 134510 (2007).

[26] T. Yokoyama and Y. Tserkovnyak, Phys. Rev. B **80**, 104416 (2009).

[27] A. F. Volkov and K. B. Efetov, Phys. Rev. Lett. **102**, 077002 (2009).

[28] M. Matsumoto, M. Koga, and H. Kusunose, J. Phys. Soc. Jpn. **81**, 033702 (2012); H. Kusunose, M. Matsumoto, and M. Koga, Phys. Rev. B **85**, 174528 (2012).

[29] C. Pfleiderer, M. Uhlarz, S. Hayden, R. Vollmer, H. v. Löhneysen, N. R. Bernhoeft, and G. G. Lonzarich, Nature (London) **412**, 58 (2001).

[30] T. Akazawa, H. Hidaka, T. Fujiwara, T. C. Kobayashi, E. Yamamoto, Y. Haga, R. Settai and Y. Onuki, J. Phy. Condens. Matter **16**, L29 (2004).

[31] W. Kohn and J. M. Lattinger, Phys. Rev. Lett. **15**, 524 (1965).

[32] N. F. Berk and J. R. Schrieffer, Phys. Rev. Lett. **17**, 433 (1966).

[33] S. Nakajima, Prog, Theor. Phys. **50**, 1101 (1973).

[34] D. Fay and J. Appel, Phys. Rev. B **22**, 3173 (1980).

[35] T. Kirkpatrick, D. Belitz, T. Vojta, and R. Narayanan, Phys. Rev. Lett. **87**, 127003 (2001).

[36] M. B. Walker and K. V. Samokhin, Phys. Rev. Lett. **88**, 207001 (2002).

[37] A. Nevidomskyy, Phys. Rev. Lett. **94**, 097003 (2005).

[38] Y. Tada, S. Fujimoto, N. Kawakami, T. Hattori, Y. Ihara, K. Ishida, K. Deguchi, N. K. Sato, and I. Satoh, J. Phys.: Conf. Ser. **449**, 012029 (2013)

[39] T. Holstein and H. Primakoff, Phys. Rev. **58**, 1098 (1940).

[40] P. Fulde and R. A. Ferrell, Phys. Rev. **135**, A550 (1964).

[41] A. I. Larkin and Yu. N. Ovchinnikov, Zh. Eksp. Teor. Fiz. **47**, 1136 (1964) [translation: Sov. Phys. JETP **20**, 762 (1965)].

[42] H. Funaki and H. Shimahara, J. Phys. Soc. Jpn. **83**, 123704 (2014); **83**, 078001 (2015).

公表論文

(1) Odd- and Even-Frequency Superconductivities
Mediated by Ferromagnetic Magnons
Hiroshi Funaki and Hiroshi Shimahara
Journal of the Physical Society of Japan **83**, 123704 (2014),
DOI: http://dx.doi.org/10.7566/JPSJ.83.123704.

Odd- and Even-Frequency Superconductivities Mediated by Ferromagnetic Magnons

Hiroshi Funaki and Hiroshi Shimahara

Department of Quantum Matter Science, ADSM, Hiroshima University, Higashi-Hiroshima 739-8530, Japan

(Received August 29, 2014; accepted October 17, 2014; published online November 21, 2014)

On the basis of a generalized Kondo-lattice model (i.e., spin-fermion model), we examine herein superconductivity mediated by magnetic excitations in ferromagnets. By applying the perturbation theory, we derive effective pairing interactions between conduction electrons. Pairing fluctuations are numerically calculated by fully accounting for the momentum and frequency dependences in quasi-one dimension. The results indicate that the normal state is unstable against even- and odd-frequency pairing fluctuations, depending on the temperature and model parameters. In a few cases, we obtain phase diagrams. The two-magnon exchange interaction is found to favor odd-frequency pairing at high temperatures (but below the ferromagnetic transition temperature); however, at low temperatures, triangle processes involving two magnons and one electron induce even- and odd-frequency pairings depending on the signs of the coupling constants of the Kondo interaction. Finally, we discuss the possibility of odd-frequency superconductivity as a bulk state in ferromagnetic superconductors.

Superconductivity mediated by magnetic fluctuations has been studied extensively in connection with exotic superconductors, such as heavy-fermion, copper oxide, organic, and iron pnictide superconductors. The features of superconductivity strongly depend on the underlying magnetic order or magnetic tendency. Superconductivity mediated by ferromagnetic fluctuations[1–6] has been studied in connection with the recently discovered ferromagnetic superconductors,[7] such as UGe_2,[8] URhGe,[9] UCoGe,[10] and $ZrZn_2$.[11] Motivated by these experimental and theoretical studies, we examine herein superconductivity mediated by ferromagnetic fluctuations using a fundamental model called the generalized Kondo-lattice model, wherein the ferromagnetic long-range order is established in a localized spin system. In particular, we illustrate the possibility of a new class of superconductivity, called odd-frequency superconductivity.[12–24]

When a long-range order is established, magnetic fluctuations are described by magnons (i.e., spin waves). The exchange of magnons between two electrons leads to an effective interaction that may induce superconductivity.[4–6,25] Interactions mediated by magnons are analogous to those mediated by phonons but have unique features: the emission and absorption of magnons by electrons depend on the spin of the electron, and a single electron can simultaneously emit and absorb magnons. The second-order processes of simultaneous emission and absorption lead to a two-magnon exchange interaction.[25] Thus, the properties of superconductivity should be quite different from those induced by phonon-mediated pairing interactions. When the underlying magnetic order is antiferromagnetic, the two-magnon exchange interaction means that either the d-wave spin singlet state or the p-wave spin triplet state is induced by the magnon-mediated interactions, depending on the electron density.[25] Karchev et al. investigated the magnon-exchange mechanism in the ferromagnetic superconductors $ZrZn_2$ and URhGe[4,5] and found that, for example, the specific heat depends linearly on the temperature at low temperatures. Hattori and Tsunetsugu examined p-wave superconductivity near a transverse saturation field by considering one-magnon exchange interaction in ferromagnetic materials.[6] In particular, they investigated the reentrant superconductivity in URhGe.

Below, we discuss how both odd- and even-frequency superconductivities are induced in ferromagnetic superconductors. The possibility of odd-frequency superconductivity was first examined by Berezinskii[12] in a study of superfluid ^{3}He. Later, some unique properties of this class of superconductivity were revealed by Balatsky and Abrahams[13] and Abrahams et al.[14] Coleman et al.[15] and Vojta and Dagotto[16] studied this state in heavy fermion compounds and triangular antiferromagnets, respectively. In recent years, considerable effort has been devoted to clarifying the features of this type of superconductivity.[17–23] Odd-frequency superconductivity in ferromagnets was studied in the context of junction systems.[19–23] Kusunose et al. examined the bulk mixed even- and odd-frequency superconductivities coexisting with ferromagnetism[24] and elucidated the emergent mixing between them.

In ferromagnetic metals, the strong exchange field suppresses antiparallel spin pairing. Therefore, for parallel spin pairing, the two-magnon exchange interaction mentioned above is simplest. However, as shown below, this interaction disappears in the limit $T \to 0$, contrary to the two-magnon exchange interaction in the antiferromagnetic case. Therefore, we also examine the third-order processes for the electron-magnon interaction, which is the lowest order for the effective interaction in the low-temperature limit.

The Hamiltonian of the generalized Kondo-lattice model is

$$H = H_t + H_J + H_{\rm K} \tag{1}$$

with

$$H_t = \sum_{i,j,\sigma} t_{ij} c^\dagger_{i\sigma} c_{j\sigma} - \mu \sum_{i,\sigma} c^\dagger_{i\sigma} c_{i\sigma}$$

$$H_J = -\sum_{(i,j)} \sum_{\alpha} J^\alpha S^\alpha_i S^\alpha_j$$

$$H_{\rm K} = \sum_{i,\alpha} \sum_{\sigma_1,\sigma_2} \frac{1}{2} J^\alpha_{\rm K} S^\alpha_i (c^\dagger_{i\sigma_1} \sigma^\alpha_{\sigma_1\sigma_2} c_{i\sigma_2}),$$

where $\alpha = x, y, z$, and σ^α denote the Pauli matrices. The summation $\sum_{\langle i,j\rangle}$ is over nearest-neighbor sites. We define $J^{\parallel} \equiv J^z \geq J^x = J^y \equiv J^{\perp} > 0$ for ferromagnets and $J_{\mathrm{K}}^{\parallel} \equiv J_{\mathrm{K}}^z$ and $J_{\mathrm{K}}^{\perp} \equiv J_{\mathrm{K}}^x = J_{\mathrm{K}}^y$.

For localized spins, we adopt the Holstein–Primakoff transformation[26] $S_i^z = S - a_i^{\dagger} a_i$ and

$$S_i^+ = \sqrt{2S}(1 - a_i^{\dagger} a_i/2S)^{1/2} a_i = (S_i^-)^{\dagger}, \tag{2}$$

below the ferromagnetic transition temperature T_{FM}. Neglecting the higher-order terms of magnon operators, we obtain the fermion-magnon model[25]

$$H = H_0 + H_1, \tag{3}$$

where

$$H_0 = \sum_{\boldsymbol{k},\sigma} \xi_{\boldsymbol{k}\sigma} c_{\boldsymbol{k}\sigma}^{\dagger} c_{\boldsymbol{k}\sigma} + \sum_{\boldsymbol{q}} \omega_{\boldsymbol{q}} a_{\boldsymbol{q}}^{\dagger} a_{\boldsymbol{q}} \tag{4}$$

and $H_1 = H_{\mathrm{K}\parallel} + H_{\mathrm{K}\perp}$, with

$$\begin{aligned} H_{\mathrm{K}\parallel} &= -\frac{J_{\mathrm{K}}^{\parallel}}{2} \sum_{\boldsymbol{k},\boldsymbol{q},\sigma} \sigma c_{\boldsymbol{k}\sigma}^{\dagger} c_{\boldsymbol{k}+\boldsymbol{q}\sigma} \left(\frac{1}{N} \sum_{\boldsymbol{q}'} a_{\boldsymbol{q}'+\boldsymbol{q}}^{\dagger} a_{\boldsymbol{q}'} - \overline{n}\delta_{\boldsymbol{q},\boldsymbol{0}} \right) \\ H_{\mathrm{K}\perp} &= J_{\mathrm{K}}^{\perp} \sqrt{\frac{S}{2N}} \sum_{\boldsymbol{k},\boldsymbol{q}} \left[a_{\boldsymbol{q}}^{\dagger} c_{\boldsymbol{k}\uparrow}^{\dagger} c_{\boldsymbol{k}+\boldsymbol{q}\downarrow} + c_{\boldsymbol{k}+\boldsymbol{q}\downarrow}^{\dagger} c_{\boldsymbol{k}\uparrow} a_{\boldsymbol{q}} \right], \end{aligned} \tag{5}$$

$\xi_{\boldsymbol{k}\sigma} = \xi_{\boldsymbol{k}}^{(0)} + h\sigma$, $h = J_{\mathrm{K}}^{\parallel}(S - \overline{n})/2$, $\overline{n} = \langle a_i^{\dagger} a_i \rangle$, $\omega_{\boldsymbol{q}} = zJ_{\parallel} S[1 - (J_{\perp}/J_{\parallel})\gamma_{\boldsymbol{q}}]$, and $\gamma_{\boldsymbol{q}} = z^{-1} \sum_{\boldsymbol{a}} e^{i\boldsymbol{q}\cdot\boldsymbol{a}}$. The quantities N and z are the number of sites and nearest-neighbor sites, respectively. If we assume $t_{ij} = -t$ for the nearest-neighbor sites (i, j) and $t_{ij} = 0$ otherwise, we obtain $\xi_{\boldsymbol{k}}^{(0)} = -zt\gamma_{\boldsymbol{k}} - \mu$. We use units in which $t = 1$.

The generalized Cooper pair operator is defined by

$$\hat{\psi}_{\sigma\bar{\sigma}}(\boldsymbol{q}, \tau_1, \tau) = (1 + \delta_{\sigma\bar{\sigma}})^{-1/2} \sum_{\boldsymbol{k}} \gamma(\boldsymbol{k}) c_{\boldsymbol{k}+\boldsymbol{q}/2,\sigma}(\tau_1) c_{-\boldsymbol{k}+\boldsymbol{q}/2,\bar{\sigma}}(\tau),$$

where $\hat{A}(\tau) = e^{\tau H} \hat{A} e^{-\tau H}$ and $\gamma(\boldsymbol{k})$ is the symmetry function to be examined. The factor $(1 + \delta_{\sigma\bar{\sigma}})^{-1/2}$ cancels the double counting when $\bar{\sigma} = \sigma$. The conventional even-frequency Cooper-pair operator is $\hat{\psi}_{\sigma\bar{\sigma}}(\boldsymbol{q}, \tau) \equiv \hat{\psi}_{\sigma\bar{\sigma}}(\boldsymbol{q}, \tau, \tau)$, whereas the odd-frequency pairing operators can be defined by

$$\hat{\phi}_{\sigma\bar{\sigma}}(\boldsymbol{q}, \tau) \equiv \left[\frac{\partial}{\partial \tau_1} \hat{\psi}_{\sigma\bar{\sigma}}(\boldsymbol{q}, \tau_1, \tau) \right]_{\tau_1=\tau}. \tag{6}$$

The even- and odd-frequency pairing susceptibilities $\chi_{\sigma\bar{\sigma}}^{(+)}$ and $\chi_{\sigma\bar{\sigma}}^{(-)}$ are defined by

$$\begin{aligned} \chi_{\sigma\bar{\sigma}}^{(+)}(\boldsymbol{q}, \tau - \tau') &= \frac{1}{N} \Big\langle T_{\tau} \left[\hat{\psi}_{\sigma\bar{\sigma}}(\boldsymbol{q}, \tau) \hat{\psi}_{\sigma\bar{\sigma}}^{\dagger}(\boldsymbol{q}, \tau') \right] \Big\rangle, \\ \chi_{\sigma\bar{\sigma}}^{(-)}(\boldsymbol{q}, \tau - \tau') &= \frac{1}{N} \Big\langle T_{\tau} \left[\hat{\phi}_{\sigma\bar{\sigma}}(\boldsymbol{q}, \tau) \hat{\phi}_{\sigma\bar{\sigma}}^{\dagger}(\boldsymbol{q}, \tau') \right] \Big\rangle, \end{aligned} \tag{7}$$

respectively. Because Eq. (6) can be rewritten as

$$\hat{\phi}_{\sigma\bar{\sigma}}(\boldsymbol{q}, \tau) = \sum_{\boldsymbol{k}} \gamma(\boldsymbol{k}) [H, c_{\boldsymbol{k}+\boldsymbol{q}/2,\sigma}(\tau)] c_{-\boldsymbol{k}+\boldsymbol{q}/2,\bar{\sigma}}(\tau), \tag{8}$$

the order parameter $\langle \hat{\phi}_{\sigma\bar{\sigma}}(\boldsymbol{q}, 0) \rangle$ involves terms proportional to the composite order parameter, such as $\langle S_{\boldsymbol{q}'}^{\alpha} \hat{\psi}_{\sigma\bar{\sigma}}(\boldsymbol{q} - \boldsymbol{q}', 0) \rangle$. We define

$$\chi_{\sigma\bar{\sigma}}^{(\pm)}(q) = \int_0^{\beta} d\tau \, e^{i\nu_m \tau} \chi_{\sigma\bar{\sigma}}^{(\pm)}(\boldsymbol{q}, \tau), \tag{9}$$

where $q \equiv (\boldsymbol{q}, i\nu_m)$ and $\nu_m = 2m\pi T$ with integer m. The divergence of the pairing susceptibility $\chi_{\sigma\bar{\sigma}}^{(\pm)}(\boldsymbol{0}, 0)$ indicates that the normal state is unstable against superconductive fluctuations with the momentum dependence $\gamma(\boldsymbol{k})$. Therefore, the instability of the normal state is signaled by the first emergence of $\gamma(\boldsymbol{k})$ for which either $\chi_{\sigma\bar{\sigma}}^{(\pm)}$ diverges. The order parameter for the superconducting state that emerges after the instability is $\langle \hat{\psi}_{\sigma\bar{\sigma}}(\boldsymbol{q}, 0) \rangle$ or $\langle \hat{\phi}_{\sigma\bar{\sigma}}(\boldsymbol{q}, 0) \rangle$. Because the instability occurs primarily at $q = 0$ (unless we consider the exceptional state, such as the Fulde-Ferrell-Larkin-Ovchinnikov state[27,28]), we examine $\chi_{\sigma\bar{\sigma}}^{(\pm)}(q = 0)$ and omit the argument q below.[29]

Green's functions for electrons and magnons are $G_{\sigma}(\boldsymbol{k}, \tau) = -\langle T_{\tau} c_{\boldsymbol{k}\sigma}(\tau) c_{\boldsymbol{k}\sigma}^{\dagger} \rangle$ and $D(\boldsymbol{q}, \tau) = -\langle T_{\tau} a_{\boldsymbol{q}}(\tau) a_{\boldsymbol{q}}^{\dagger} \rangle$, respectively. We define $G_{\sigma}(\boldsymbol{k}, i\omega_n)$ and $D(\boldsymbol{q}, i\nu_m)$ in a standard manner, where $\omega_n = (2n + 1)\pi T$ and n is an integer. In this work, we ignore the self-energies in G_{σ} and D for simplicity.

The unperturbed pairing susceptibility is expressed as

$$\chi_{0\sigma\bar{\sigma}}^{(\pm)} = (T/N) \sum_{k} |\gamma_{\pm}(k)|^2 w_{\sigma\bar{\sigma}}(k),$$

where $\gamma_+(k) = \gamma(\boldsymbol{k})$, $\gamma_-(k) = \omega_n \gamma(\boldsymbol{k})$, and $w_{\sigma\bar{\sigma}}(k) = G_{\sigma}(k) G_{\bar{\sigma}}(-k)$, with $k \equiv (\boldsymbol{k}, i\omega_n)$ and $k' \equiv (\boldsymbol{k}', i\omega_{n'})$. The reducible vertex part $\Gamma_{\sigma\bar{\sigma}}^{\mathrm{red}}$ is defined by

$$\chi_{\sigma\bar{\sigma}}^{(\pm)} = \chi_{0\sigma\bar{\sigma}}^{(\pm)} + \frac{T^2}{N^2} \sum_{k,k'} \gamma_{\pm}(k) w_{\sigma\bar{\sigma}}(k) \, \Gamma_{\sigma\bar{\sigma}}^{\mathrm{red}}(k, k') w_{\sigma\bar{\sigma}}(k') \, \gamma_{\pm}^*(k'),$$

and is expressed in terms of the irreducible part $\Gamma_{\sigma\bar{\sigma}}$ as

$$\hat{\Gamma}_{\sigma\bar{\sigma}}^{\mathrm{red}} = \hat{\Gamma}_{\sigma\bar{\sigma}} + \hat{\Gamma}_{\sigma\bar{\sigma}} \hat{W}_{\sigma\bar{\sigma}} \hat{\Gamma}_{\sigma\bar{\sigma}}^{\mathrm{red}} = \hat{\Gamma}_{\sigma\bar{\sigma}} \Big[\boldsymbol{1} - \hat{W}_{\sigma\bar{\sigma}} \hat{\Gamma}_{\sigma\bar{\sigma}} \Big]^{-1}, \tag{10}$$

in matrix form, where $\hat{\Gamma}_{\sigma\bar{\sigma}}^{\mathrm{red}}$, $\hat{\Gamma}_{\sigma\bar{\sigma}}$, and $\hat{W}_{\sigma\bar{\sigma}}$ are matrices whose elements are $\Gamma_{\sigma\bar{\sigma}}^{\mathrm{red}}(k, k')$, $\Gamma_{\sigma\bar{\sigma}}(k, k')$, and $(T/N)\delta_{kk'} w_{\sigma\bar{\sigma}}(k)$, respectively ($\boldsymbol{1}$ is the identity matrix).

We also define the row vector $\hat{\gamma}_{\pm}$ whose element is $\gamma_{\pm}(k)$, and $\hat{v}_{\pm} = \hat{\gamma}_{\pm} \hat{W}_{\sigma\bar{\sigma}}^{1/2}$. Thus, we obtain $\chi_{0\sigma\bar{\sigma}}^{(\pm)} = \hat{\gamma}_{\pm} \hat{W}_{\sigma\bar{\sigma}} \hat{\gamma}_{\pm}^{\dagger}, = \hat{v}_{\pm} \hat{v}_{\pm}^{\dagger}$, and

$$\chi_{\sigma\bar{\sigma}}^{(\pm)} = \hat{v}_{\pm} \Big[\boldsymbol{1} - \hat{\Lambda}_{\sigma\bar{\sigma}} \Big]^{-1} \hat{v}_{\pm}^{\dagger}, \tag{11}$$

where $\Lambda_{\sigma\bar{\sigma}} = \hat{W}_{\sigma\bar{\sigma}}^{1/2} \hat{\Gamma}_{\sigma\bar{\sigma}} \hat{W}_{\sigma\bar{\sigma}}^{1/2}$. We next consider the eigenequation

$$\hat{\Lambda}_{\sigma\bar{\sigma}} \hat{v} = \lambda \hat{v}, \tag{12}$$

where λ and $\hat{v}$ are the largest eigenvalue and the corresponding eigenvector, respectively. We write the element of $\hat{v}$ as $v(k)$. When $\lambda < 1$, the pairing susceptibilities are positive and finite for any $\gamma(k)$. Thus, in this case, the system is in the normal state. When varying a parameter such as the temperature in the normal state, if $\lambda \to 1$ and $\hat{v}_{\pm}$ has a component proportional to $\hat{v}$, the pairing susceptibility diverges as $\chi_{\sigma\bar{\sigma}}^{(\pm)} \sim (1 - \lambda)^{-1} \to \infty$. This implies a phase transition to the superconducting state, as mentioned above.

The vertex part can be divided into two parts as

$$\Gamma_{\sigma\bar{\sigma}}(k, k') = \Gamma_{\sigma\bar{\sigma}}^{(+)}(k, k') + \Gamma_{\sigma\bar{\sigma}}^{(-)}(k, k'), \tag{13}$$

where

$$\begin{aligned} \Gamma_{\sigma\bar{\sigma}}^{(\pm)}((\boldsymbol{k}, i\omega_n), (\boldsymbol{k}', i\omega_{n'})) &= \pm \Gamma_{\sigma\bar{\sigma}}^{(\pm)}((\boldsymbol{k}, -i\omega_n), (\boldsymbol{k}', i\omega_{n'})) \\ &= \pm \Gamma_{\sigma\bar{\sigma}}^{(\pm)}((\boldsymbol{k}, i\omega_n), (\boldsymbol{k}', -i\omega_{n'})). \end{aligned} \tag{14}$$

Because $w_{\sigma\bar{\sigma}}(k)$ is an even function of ω_n, only $\Gamma_{\sigma\bar{\sigma}}^{(+)}$ and $\Gamma_{\sigma\bar{\sigma}}^{(-)}$ contribute to $\chi_{\sigma\bar{\sigma}}^{(+)}$ and $\chi_{\sigma\bar{\sigma}}^{(-)}$, respectively.

Figure 1 shows the Feynman diagrams that contribute to the vertex part. Figure 1(a) depicts the one-magnon exchange interaction

$$\Gamma^{(1)}_{\sigma,-\sigma} = \frac{1}{4} {J_{\mathrm{K}}^{\perp}}^2 D(-\sigma(k+k')) \tag{15}$$

analogous to the phonon-mediated interaction; however, this interaction contributes only to antiparallel spin pairing.

The two-magnon exchange interaction, depicted in Fig. 1(b), is written as

$$\begin{aligned}\Gamma^{(2)}_{\sigma\bar{\sigma}} &= \sigma\bar{\sigma}\frac{{J_{\mathrm{K}}^{\parallel}}^2}{4}\frac{T}{N}\sum_{k_1} D(k_1-k')D(k_1-k)\\ &= -\sigma\bar{\sigma}\frac{{J_{\mathrm{K}}^{\parallel}}^2}{4}\frac{1}{N}\sum_{\boldsymbol{k}_1}\frac{[n(\omega_{\boldsymbol{k}_1-\boldsymbol{k}'})-n(\omega_{\boldsymbol{k}_1-\boldsymbol{k}})](\omega_{\boldsymbol{k}_1-\boldsymbol{k}'}-\omega_{\boldsymbol{k}_1-\boldsymbol{k}})}{\nu^2_{n'-n}+(\omega_{\boldsymbol{k}_1-\boldsymbol{k}'}-\omega_{\boldsymbol{k}_1-\boldsymbol{k}})^2},\end{aligned} \tag{16}$$

where $n(\omega)$ is the Bose distribution function. This interaction contributes to both antiparallel and parallel spin pairings.[30] In the ferromagnetic case, $\Gamma^{(2)}_{\sigma\bar{\sigma}} \to 0$ in the limit $T \to 0$, because $n(\omega_{\boldsymbol{q}}) \to 0$, in contrast to the antiferromagnetic case.[25]

The triangular diagrams depicted in Figs. 1(c) and 1(d) correspond to triangle processes, which involve two magnons and one electron, and give rise to the effective interactions

$$\begin{aligned}\Gamma^{(3)}_{\sigma\bar{\sigma}} = -\frac{J_{\mathrm{K}}^{\parallel}{J_{\mathrm{K}}^{\perp}}^2}{8}\frac{T}{N}\sum_{k_1}\Big[&\bar{\sigma}G_{-\sigma}(k_1)D(\sigma(k_1-k))D(\sigma(k_1-k'))\\ &+\sigma G_{-\bar{\sigma}}(-k_1)D(\bar{\sigma}(k-k_1))D(\bar{\sigma}(k'-k_1))\Big].\end{aligned}$$

For parallel spin pairing, we obtain

$$\begin{aligned}\Gamma^{(3)}_{\sigma\sigma} = -\frac{J_{\mathrm{K}}^{\parallel}{J_{\mathrm{K}}^{\perp}}^2}{4}\frac{1}{N}\sum_{\boldsymbol{k}_1}\Bigg[&f(\sigma\xi_{\boldsymbol{k}_1-\sigma})\\ &\times\frac{(\sigma\xi_{\boldsymbol{k}_1-\sigma}-\omega_{\boldsymbol{k}_1-\boldsymbol{k}})(\sigma\xi_{\boldsymbol{k}_1-\sigma}-\omega_{\boldsymbol{k}_1-\boldsymbol{k}'})-\omega_n\omega_{n'}}{[\omega_n^2+(\sigma\xi_{\boldsymbol{k}_1-\sigma}-\omega_{\boldsymbol{k}_1-\boldsymbol{k}})^2][\omega_{n'}^2+(\sigma\xi_{\boldsymbol{k}_1-\sigma}-\omega_{\boldsymbol{k}_1-\boldsymbol{k}'})^2]}\\ &-\frac{n(\omega_{\boldsymbol{k}_1-\boldsymbol{k}})\begin{pmatrix}(\sigma\xi_{\boldsymbol{k}_1-\sigma}-\omega_{\boldsymbol{k}_1-\boldsymbol{k}})\\ \times(\omega_{\boldsymbol{k}_1-\boldsymbol{k}'}-\omega_{\boldsymbol{k}_1-\boldsymbol{k}})+\omega_n\nu_{n'-n}\end{pmatrix}}{[\omega_n^2+(\sigma\xi_{\boldsymbol{k}_1-\sigma}-\omega_{\boldsymbol{k}_1-\boldsymbol{k}})^2][\nu^2_{n'-n}+(\omega_{\boldsymbol{k}_1-\boldsymbol{k}'}-\omega_{\boldsymbol{k}_1-\boldsymbol{k}})^2]}\\ &+\frac{n(\omega_{\boldsymbol{k}_1-\boldsymbol{k}'})\begin{pmatrix}(\sigma\xi_{\boldsymbol{k}_1-\sigma}-\omega_{\boldsymbol{k}_1-\boldsymbol{k}'})\\ \times(\omega_{\boldsymbol{k}_1-\boldsymbol{k}'}-\omega_{\boldsymbol{k}_1-\boldsymbol{k}})+\omega_{n'}\nu_{n'-n}\end{pmatrix}}{[\omega_{n'}^2+(\sigma\xi_{\boldsymbol{k}_1-\sigma}-\omega_{\boldsymbol{k}_1-\boldsymbol{k}'})^2][\nu^2_{n'-n}+(\omega_{\boldsymbol{k}_1-\boldsymbol{k}'}-\omega_{\boldsymbol{k}_1-\boldsymbol{k}})^2]}\Bigg].\end{aligned} \tag{17}$$

Based on Eqs. (16) and (17), both $\Gamma^{(2)}_{\sigma\sigma}$ and $\Gamma^{(3)}_{\sigma\sigma}$ contribute to the odd-frequency part $\Gamma^{(-)}_{\sigma\sigma}$ and may induce odd-frequency superconductivity. In the following, we illustrate this result in one dimension through a numerical calculation.[31] The Fermi-surface splitting due to the exchange field $h\sigma$ is disadvantageous to antiparallel spin pairing. In particular, when h is sufficiently large, antiparallel spin pairing is suppressed. Therefore, we focus on parallel spin pairing in this study.[32] Hereafter, we call the even-frequency odd-parity state the EOT state and the odd-frequency even-parity state the OET state. As an example, we examine the case in which $J_\perp/J_\parallel = 0.95$, $J_\parallel = 0.01$, and $\mu = 0$. Because of particle-hole symmetry, the pairing susceptibility for two spin-up electrons is the same as that for two spin-down electrons when $\mu = 0$.

Figure 2 shows $1-\lambda$ as a function of temperature and the profile of $\Delta(k) \equiv v(k)/\sqrt{w_{\downarrow\downarrow}(k)}$ for isotropic Kondo coupling ($J_{\mathrm{K}}^{\perp} = J_{\mathrm{K}}^{\parallel} \equiv J_{\mathrm{K}}$). The eigenvector $v(k)$ is for $\Lambda_{\downarrow\downarrow}$, and the eigenvalues λ are identical for $\uparrow\uparrow$ pairs and $\downarrow\downarrow$ pairs. In Fig. 2(a), the normal state is stable against pairing fluctuations where $1-\lambda > 0$, but becomes unstable where the curves cross the line $1-\lambda = 0$. In the region where $1-\lambda < 0$, the perturbation theory breaks down. At $J_{\mathrm{K}} = 0.9$, the OET state occurs in the high-temperature region, whereas, at $J_{\mathrm{K}} = -0.9$, the EOT state occurs in both the high- and low-temperature regions. The unusual reentrant transitions to the superconducting states are due to the strong temperature dependence of the vertex parts involving the Bose distribution functions of the magnons. Because the structure of $\Delta(k)$ at $\lambda = 1$ reflects the structure of the order parameter near the transition temperature, Fig. 2(b) suggests that the order parameters have a peak near the Fermi momentum ($p_{\mathrm{F}\downarrow} \approx 0.50\pi$).

Figure 3 shows the phase diagram in the J_{K}–T plane for isotropic Kondo coupling. The phase boundaries are determined from the condition $\lambda = 1$. Except near $J_{\mathrm{K}} = 0$, the superconductivity occurs in both the high- and low-temperature regions. The OET and EOT states occur for $J_{\mathrm{K}} > 0$ and $J_{\mathrm{K}} < 0$, respectively. The asymmetry with respect to the sign of J_{K} originates from the third-order term $\Gamma^{(3)}_{\sigma\sigma}$. The normal phase in the intermediate temperature region can be reached

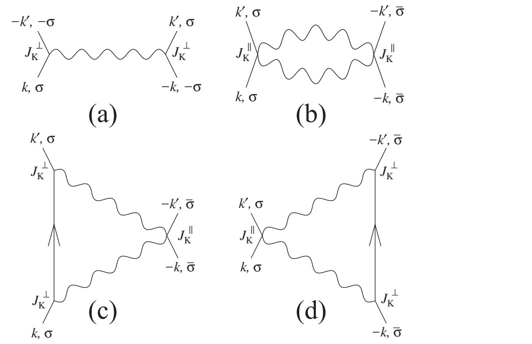

Fig. 1. Feynman diagrams that contribute to the vertex part $\Gamma_{\sigma\bar{\sigma}}(k,k')$. The solid and wavy lines correspond to the electron and magnon Green's functions, respectively.

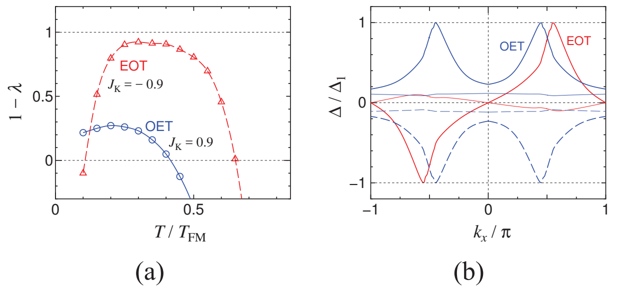

Fig. 2. (Color online) (a) Minimum eigenvalue $1-\lambda$ as a function of temperature T, and (b) profile of $\Delta(k_x, \omega_n)$ at the superconducting transition temperature. The isotropic Kondo coupling $J_{\mathrm{K}}^{\parallel} = J_{\mathrm{K}}^{\perp} = J_{\mathrm{K}}$ is assumed. The red and blue curves show the results for the EOT and OET states, respectively. In panel (a), the open circle and solid curve show the results for $J_{\mathrm{K}} = 0.9$, whereas the open triangle and dashed curve show the results for $J_{\mathrm{K}} = -0.9$. In panel (b), J_{K} values of -0.31 and 0.28 are assumed for the EOT and OET states, respectively. These values give $\lambda = 1$ at $T = 0.8T_{\mathrm{FM}}$. The thick and thin solid curves show the results for $\omega_n = \pi T$ and $3\pi T$, whereas the thick and thin dashed curves show those for $\omega_n = -\pi T$ and $-3\pi T$, respectively. Δ_1 is the magnitude of the peak value for $\omega_n = \pm\pi T$. For the EOT state, the results for $\omega_n = -\pi T$ and $-3\pi T$ coincide with those for $\omega_n = \pi T$ and $3\pi T$, respectively.

from the high-temperature normal phase, through the blue region.

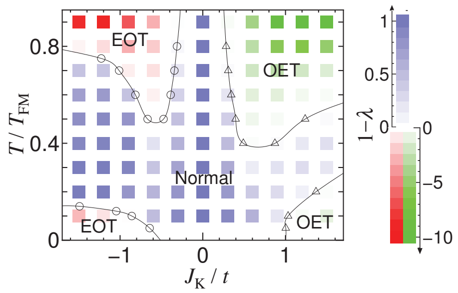

Fig. 3. (Color online) Phase diagram in $J_{\rm K}$–T plane for isotropic Kondo coupling. The squares are color-coded to represent the value of $1 - \lambda$ at the center of the square. The color scale is displayed on the right of the figure. The open circles and triangles show the points at which $\lambda = 1$. At the center of each red square and each open circle, the minimum eigenvalue occurs for EOT pairing. At the center of each green square and each open triangle, the minimum eigenvalue occurs for OET pairing. The solid curves are the phase boundaries deduced from these results. In the region near $J_{\rm K} = 0$, antiparallel spin pairing may occur.[33)]

Figure 4 shows the result when the Kondo coupling is Ising-like ($J_{\rm K}^{\perp} = 0$). The OET state occurs over very large areas of parameter space, but not the EOT state. Because $\Gamma^{(3)}_{\sigma\sigma} = 0$ in this case, the OET state occurs due to the two-magnon exchange interaction $\Gamma^{(2)}_{\sigma\sigma}$. In this phase diagram, antiparallel spin pairing does not occur even when $|J_{\rm K}^{\parallel}|$ is small, because $\Gamma^{(1)}_{\sigma,-\sigma} = \Gamma^{(3)}_{\sigma,-\sigma} = 0$ and $\Gamma^{(2)}_{\sigma,-\sigma}$ is repulsive.

We can take the results shown in Fig. 4 as those for isotropic Kondo coupling where $\Gamma^{(3)}_{\sigma\sigma}$ is ignored, because the condition $J_{\rm K}^{\perp} = 0$ eliminates $\Gamma^{(3)}_{\sigma\sigma} \propto J_{\rm K}^{\parallel} J_{\rm K}^{\perp 2}$ from the theory without any other change. Therefore, the appearance of the EOT state in Fig. 3 is due to triangle processes.

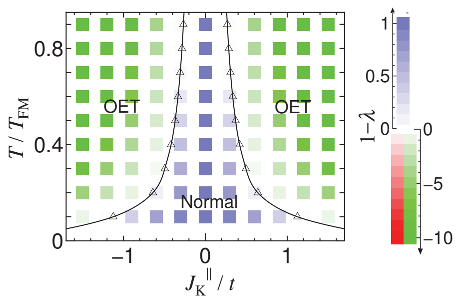

Fig. 4. (Color online) Similar to Fig. 3, but shows the phase diagram in the $J_{\rm K}^{\parallel}$–T plane, for Ising-like Kondo coupling ($J_{\rm K}^{\perp} = 0$).

Figure 5 shows the phase diagram at $T = 0.5T_{\rm FM}$. The superconducting areas are large near the Ising line $J_{\rm K}^{\perp} = 0$. The EOT state occurs only when $J_{\rm K}^{\parallel} < 0$, but near the Ising line this state is suppressed by the emergence of the OET state. Note that, where $J_{\rm K}^{\parallel} < 0$, the real phase boundaries between the EOT and OET states should be displaced from those shown in Fig. 5 because they are determined by comparing the pairing susceptibilities for the normal state. In this phase diagram, antiparallel spin pairing is ignored.[34)]

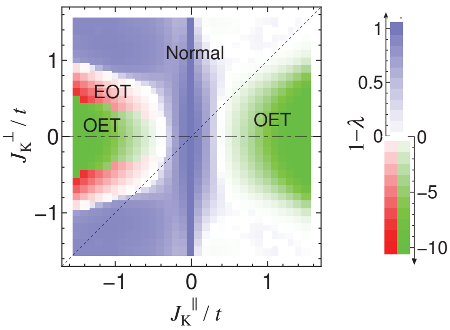

Fig. 5. (Color online) Similar to Fig. 3, but shows the phase diagram in the $J_{\rm K}^{\parallel}$–$J_{\rm K}^{\perp}$ plane at $T = 0.5T_{\rm FM}$. The Kondo couplings on the dotted and dot-dashed lines are isotropic and Ising-like, respectively.

To summarize, both the two-magnon exchange processes and the triangle processes contribute to the odd- and even-frequency pairings. At higher temperatures but below $T_{\rm FM}$, both processes are pronounced because of the high magnon density. As a result, either the OET or EOT state occurs over large areas of parameter space. The OET state is favored by uniaxial Kondo coupling through the two-magnon exchange interaction. At low temperatures, however, only triangle processes remain: these can induce either of the two states depending on the parameter values.

The self-energy effect would decrease the area in parameter space where superconductivity occurs and could change the phase diagrams. Furthermore, the phase diagrams in two and three dimensions would be different from those obtained above. These problems are left for future research.

In conclusion, we derived an effective pairing interaction mediated by magnons in ferromagnetic superconductors, taking into account triangle processes as well as two-magnon exchange processes. These interactions are illustrated in one dimension and found to induce either odd- or even-frequency superconductivity. The present system is thus a candidate for odd-frequency superconductivity in a bulk homogeneous state.

1) D. Fay and J. Appel, Phys. Rev. B **22**, 3173 (1980).
2) T. Kirkpatrick, D. Belitz, T. Vojta, and R. Narayanan, Phys. Rev. Lett. **87**, 127003 (2001).
3) M. B. Walker and K. V. Samokhin, Phys. Rev. Lett. **88**, 207001 (2002).
4) N. I. Karchev, K. B. Blagoev, K. S. Bedell, and P. B. Littlewood, Phys. Rev. Lett. **86**, 846 (2001).
5) N. Karchev, Phys. Rev. B **67**, 054416 (2003).
6) K. Hattori and H. Tsunetsugu, Phys. Rev. B **87**, 064501 (2013).
7) D. Aoki and J. Flouquet, J. Phys. Soc. Jpn. **81** 011003 (2012).
8) S. Saxena, P. Agarwal, K. Ahilan, F. M. Grosche, R. Haselwimmer, M. Steiner, E. Pugh, I. Walker, S. Julian, P. Monthoux, G. Lonzarich, A. Huxley. I. Sheikin, D. Braithwaite, and J. Flouquet, Nature (London) **406**, 587 (2000).
9) D. Aoki, A. Huxley, E. Ressouche, D. Braithwaite, J. Flouquet, J.-P. Brison, E. Lhotel, and C. Paulsen, Nature (London) **413**, 613 (2001).
10) N. T. Huy, A. Gasparini, D. E. de Nijs, Y. Huang, J. C. P. Klaasse, T. Gortenmulder, A. de Visser, A. Hamann, T. Görlach, and H. v. Löhneysen, Phys. Rev. Lett. **99**, 067006 (2007).
11) C. Pfleiderer, M. Uhlarz, S. Hayden, R. Vollmer, H. v. Löhneysen, N. R. Bernhoeft, and G. G. Lonzarich, Nature (London) **412**, 58 (2001).
12) V. L. Berezinskii, Pis'ma Zh. Eksp. Teor. Fiz. **20**, 628 (1974) [translation: Sov. Phys. JETP, **20**, 287 (1974)].

13) A. Balatsky and E. Abrahams, Phys. Rev. B **45**, 13125 (1992).
14) E. Abrahams, A. Balatsky, D. J. Scalapino, and J. R. Schrieffer, Phys. Rev. B **52**, 1271 (1995).
15) P. Coleman, E. Miranda, and A. Tsvelik, Phys. Rev. Lett. **70**, 2960 (1993); Phys. Rev. B **49**, 8955 (1995).
16) M. Vojta and E. Dagotto, Phys. Rev. B **59**, 713 (1999).
17) D. Solenov, I. Martin, and D. Mozyrsky, Phys. Rev. B **79**, 132502 (2009).
18) H. Kusunose, Y. Fuseya, and K. Miyake, J. Phys. Soc. Jpn. **80**, 054702 (2011).
19) F. S. Bergeret, A. F. Volkov, and K. B. Efetov, Phys. Rev. Lett. **86**, 4096 (2001); Rev. Mod. Phys. **77**, 1321 (2005).
20) Y. Asano, Y. Sawa, Y. Tanaka, and A. A. Golubov, Phys. Rev. B **76**, 224525 (2007).
21) T. Yokoyama, Y. Tanaka, and A. A. Golubov, Phys. Rev. B **75**, 134510 (2007).
22) T. Yokoyama and Y. Tserkovnyak, Phys. Rev. B **80**, 104416 (2009).
23) A. F. Volkov and K. B. Efetov, Phys. Rev. Lett. **102**, 077002 (2009).
24) H. Kusunose, M. Matsumoto, and M. Koga, Phys. Rev. B **85**, 174528 (2012); M. Matsumoto, M. Koga, and H. Kusunose, J. Phys. Soc. Jpn. **81**, 033702 (2012).
25) H. Shimahara, J. Phys. Soc. Jpn. **63**, 1861 (1994).
26) T. Holstein and H. Primakoff, Phys. Rev. **58**, 1098 (1940).
27) P. Fulde and R. A. Ferrell, Phys. Rev. **135**, A550 (1964).
28) A. I. Larkin and Yu. N. Ovchinnikov, Zh. Eksp. Teor. Fiz. **47**, 1136 (1964) [translation, Sov. Phys. JETP **20**, 762 (1965)].
29) In most known cases, oscillating states ($q \neq 0$) are energetically unfavorable, but their possibility cannot be excluded when $h \sim \Delta_0$, where Δ_0 denotes the superconductive energy gap.
30) In one dimension, $\Gamma^{(2)}_{\sigma\sigma}$ is attractive, whereas $\Gamma^{(2)}_{\sigma,-\sigma}$ is repulsive, for two electrons near the Fermi surface, because of the factor $\sigma\bar{\sigma}$.
31) Even in one dimension, small interchain coupling should be implicitly assumed for the spontaneous symmetry breaking at finite temperature. In this sense, the system examined here is quasi-one-dimensional.
32) Where $|J^{\parallel}_{\mathrm{K}}|$ is small or near T_{FM}, h is small, and thus antiparallel spin pairing may occur *a priori*, which will be examined in a separate paper.
33) Near $J^{\parallel}_{\mathrm{K}} = 0$, $\Gamma^{(1)}_{\sigma,-\sigma}$ may induce antiparallel spin pairing at low temperatures such that the repulsive $\Gamma^{(2)}_{\sigma,-\sigma}$ is small. In Fig. 3, however, if $|J^{\parallel}_{\mathrm{K}}| \gtrsim 0.1t$, $|h|$ is sufficiently large to suppress antiparallel spin pairing, because, since $T_{\mathrm{c}} \lesssim T_{\mathrm{FM}} = 0.0024t$, $|h| = |J^{\parallel}_{\mathrm{K}}|(S - \bar{n})/2 \sim 0.25|J_{\mathrm{K}}| \gtrsim 0.025t \gg T_{\mathrm{c}}$.
34) In the region where $|J^{\parallel}_{\mathrm{K}}|$ is small and $|J^{\perp}_{\mathrm{K}}|$ is large, $\Gamma^{(1)}_{\sigma,-\sigma}$ may induce antiparallel spin pairing. When $|J^{\perp}_{\mathrm{K}}|$ is small, $|J^{\parallel}_{\mathrm{K}}| \gtrsim 0.1t$ is sufficiently large to suppress antiparallel spin pairing, similar to the condition for Fig. 3. As $|J^{\perp}_{\mathrm{K}}|$ increases, the lower limit of $|J^{\parallel}_{\mathrm{K}}|$ increases. The construction of a complete phase diagram including both parallel and antiparallel spin pairings is left for future research.